

DRAFT

Report of the NSLS-II Stability Task Force

Table of Contents

1. Executive Summary
2. General NSLS-II Beamline Stability Guidelines
3. Stability Requirements for NSLS-II Beamlines
4. Conventional Construction
5. Mechanical Systems
6. Orbit Feedback
7. Electrical Systems
8. RF System

1. Executive Summary

The NSLS-II has been designed to provide ultra high-brightness x-ray sources. The storage ring is comprised of 30 double-bend-achromatic cells and has 15 superperiods. The insertion device straight sections have lengths 6m (low betax and betay) and 8m (high betax and low betay). The lattice without insertion devices has 2nm-horizontal emittance. Damping wigglers will be used to reduce the horizontal emittance below 1nm. The vertical emittance is chosen to be the diffraction limit for 1 Angstrom radiation, i.e. 8pm.

To realize the benefits of the high brightness and small beam sizes of NSLS-II, it is essential that the photon beams are exceedingly stable in position and angle. For timing experiments, it is also necessary that the arrival-time jitter of the bunch be small. We shall require transverse beam motion to be less than 10% of beamsize or angular spread, and longitudinal beam motion to be less than 5% of equilibrium bunch duration. Ideally, the temporal, spatial and angular stability of the electron beam should be maintained for at least the duration of spectral scans, which typically run from a few ms to a few hours.

$$\begin{aligned}\Delta x &< 0.1\sqrt{\beta_x \varepsilon_x + \eta^2 \sigma_p^2} & \Delta x' &< 0.1\sqrt{\varepsilon_x / \beta_x + \eta'^2 \sigma_p^2} \\ \Delta y &< 0.1\sqrt{\beta_y \varepsilon_y} & \Delta y' &< 0.1\sqrt{\varepsilon_y / \beta_y} \\ \Delta t &< 0.05 \sigma_t & \Delta p / p &< 0.05 \sigma_p\end{aligned}$$

Our philosophy is to follow best engineering practices to optimize the passive stability of the facility within reasonable cost. Active orbit feedback will be used to achieve the very high level of stability required by the users.

We shall employ top-off injection which produces stable heating from the electron beam. At a particular location in the storage ring tunnel the temperature will be regulated to $\pm 0.1^\circ C$. On the experimental floor temperature regulation to $\pm 0.5^\circ C$ will be sufficient. Temperatures of the experimental beamlines and end-stations can be held to tighter tolerance as required by the individual research programs.

Great care must be taken in the design to isolate the concrete floor from roof supports and from vibrating mechanical equipment. The goal is to keep vertical floor motion below 25nm in the frequency bandwidth 4-50 Hz, where the motion is expected to be uncorrelated. The magnets will be placed on specially designed girders which have no resonance below 50 Hz, so there will be negligible amplification of vibration amplitude from the floor to the top of the girder for frequency below 50 Hz. Floor motion falls off fast at higher frequency ($\sim 1/\omega^4$). Even if there is some amplification by the girder above 50 Hz the effect on the electron beam is expected to be small. The floor motion at frequencies below 4 Hz can be significantly larger. The effect on the electron beam of vibrations with frequency below 4 Hz is reduced since the associated wavelength is long and major portions of the storage ring containing many girders move together. However,

we can expect significant motion of the electron beam with frequency below 4 Hz that will need to be reduced by feedback.

There is an amplification factor between quadrupole displacement and the movement of the electron beam. Quadrupoles vibrating randomly and independently with rms amplitude of 25 nm will generate electron orbit motion with rms amplitude ~ 350 nm at a location with unit beta function. Since the quadrupoles on a girder move in a correlated manner, random and independent motion of the girders with rms amplitude of 25 nm will generate less motion of the orbit (~ 120 nm at a location with unit betafunction) than would independent motion of the quadrupoles.

Dipole, quadrupole and sextupole power supply stability requirements are within standard achievable limits (< 50 ppm for dipoles and < 100 ppm for multipoles). With a well-corrected orbit having less than $100 \mu m$ displacement in the quadrupole magnets, the quadrupole power supply variation will produce $< 0.2 \mu m$ motion of the electron beam. Variation in the dipole field ($\Delta B/B$) will cause a motion of the electron beam, $\eta(\Delta B/B)$, where η is the storage ring dispersion. At a location with $\eta \sim 0.1 m$, the horizontal motion of the electron beam will be $5 \mu m$. Since the fractional energy spread $\sigma_p \sim 10^{-3}$, the beam size at this location is $> 100 \mu m$. The variation in the dipole field will result in a variation in the average electron energy which will result in an arrival-time jitter of $< 5\%$ of the equilibrium bunch duration.

The tightest orbit tolerance is required at the undulator sources located in the 5m-long low-beta insertions. The rms vertical beam size is $3 \mu m$ at these locations and the rms vertical angular spread is $3 \mu rad$. Therefore, we must hold the electron orbit constant to $\pm 0.3 \mu m$ at the beam position monitors (BPMs), separated by 5m, bounding the straight section. A temperature variation of $\pm 0.1^\circ C$ will produce $\pm 1.1 \mu m$ motion of the BPM if it is supported from the floor by 1 m of structural steel. Therefore, the BPMs bounding the undulator straights must be supported by stands made from materials with low coefficient of thermal expansion, or by thermally stabilized steel stands. Our goal is to have the thermal motion no greater than $\pm 0.1 \mu m$ vertically and $\pm 1 \mu m$ horizontally. The other BPMs around the ring will be incorporated into the aluminum chamber. Consideration is being given to the possibility of constraining them with invar, so that they also can be held fixed vertically to better than $0.2 \mu m$.

The design of the RF BPMs uses the Libera digital processors. For the BPMs bounding the low-beta insertions, our goal is to achieve a measurement precision of $0.1 \mu m$ within 100 Hz bandwidth. This is about a factor of 2 better than the present state-of-the art. The use of x-ray BPMs on the user beamlines is also envisioned. The question of whether we should implement the Decker lattice distortion to eliminate contamination of the undulator output is under consideration.

The quadrupoles and sextupoles will be aligned on girders to better than $50 \mu m$, and girders will be aligned relative to each other to better than $100 \mu m$. Beam-based alignment will be used to calibrate the BPMs relative to the quadrupoles and sextupoles. The orbit correction system contains 7 correction magnets and 7 BPMs per period. It has the capability of correcting the misalignment expected during first commissioning of the storage ring as well as for the long-term settlement of the concrete floor (estimated to be $10 \mu m/10 m/year$).

The orbit feedback system uses a subset of 4 BPMs and 4 correction dipoles per cell ($\times 30$). These correction dipoles are located over stainless steel chambers so the feedback correction bandwidth is greater than 60 Hz. The correction dipoles will be driven by the sum of two signals, one slow with the ability to drive the power supply to the maximum strength of $800 \mu rad$ and the other fast with the strength falling off at higher frequency. The resolution of the last bit is $0.01 \mu rad$ and the noise level is $0.003 \mu rad$. This corresponds to 4ppm of $800 \mu rad$.

2. General NSLS-II Beamline Stability Guidelines

The electron beam sizes and angular divergences for selected NSLS-II sources, including insertion device straight sections, bending magnets, and three-pole wigglers, is provided in Table 2.1.

Table 2.1. Electron Beam Sizes and Divergences for selected NSLS-II sources

Type of source	5 m straight section	8 m straight section	Bend magnet *	1T three-pole wiggler
σ_x [μm]	38.5	99.5	44.2 (35.4-122)	136
$\sigma_{x'}$ [μrad]	14.2	5.48	63.1 (28.9-101)	14.0
σ_y [μm]	3.05	5.51	15.7	15.7
$\sigma_{y'}$ [μrad]	3.22	1.78	0.63	0.62

The size and angular divergence of photon beams from NSLS-II insertion devices, as a function of photon energy, are shown in Figs. 2.1 and 2.2. Both the source size and source divergence values diverge from the diffraction-limited value above ~ 1 keV photon energy, owing to the quadrature contribution of the electron beam size and angular divergence. In general, the beamlines which provide the most stringent requirements on beam stability are those that accept only the diffraction-limited portion of the photon beams. Above ~ 1 keV, overfilling of a diffraction-limited beamline acceptance (both space and angle) provides a degree of tolerance to beam motion. Below ~ 1 keV, the photon beam is diffraction-limited in the vertical and there is less fractional tolerance to beam motion in that direction. The absolute stability requirements on the electron beam should be determined at high photon energy, where the diffraction-limited photon phase space is smallest. We propose the following electron beam stability requirements: spatial stability = 10% of U19 CPMU (in 5m ID straight) photon beam size at high energy (50 keV), angular = 10% of U19 divergence at high energy (50 keV):

- vert. position: 10% of 3 micron = 0.3 micron
- vert. angle: 10% of 7 microradian = 0.7 microradian
- horiz. position: 10% of 40 micron = 4.0 micron
- horiz. angle: 10% of 15 microradian = 1.5 microradian

The corresponding fractions of the electron beam size in the 5m ID straight sections are:

- vertical position: 0.3 micron / 3 micron = 10%
- vertical angle: 0.7 microradian / 3 microradian = 24%
- horizontal position: 4.0 micron / 40 micron = 10%
- horizontal angle: 1.5 microradian / 15 microradian = 10%

Since some beamline experiments may need greater stability than the values quoted above, consider a "stretch" goal which is 3 times tighter, i.e.

- vert. position: 0.1 micron / 3 micron = 3% of vert. ebeam size
- vert. angle: 0.2 microradian / 3 microradian = 7% of vert. ebeam divergence
- horiz. position: 1.3 micron / 40 micron = 3% of horiz. ebeam size
- horiz. angle: 0.5 microradian / 15 microradian = 3% of horiz. ebeam divergence

Time dependence: Ideally, the spatial and angular stability of the electron beam should be maintained for at least the duration of spectral scans, which typically run from a few ms to a few hours.

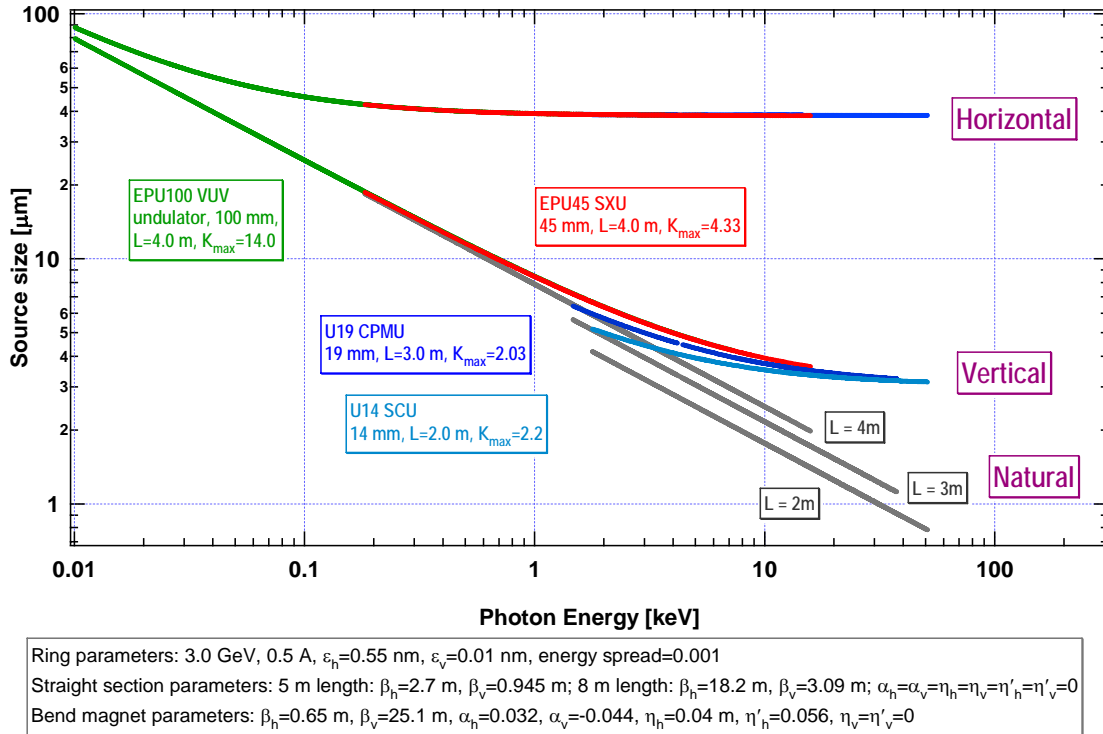


Figure 2.1: Source Size vs Photon Energy

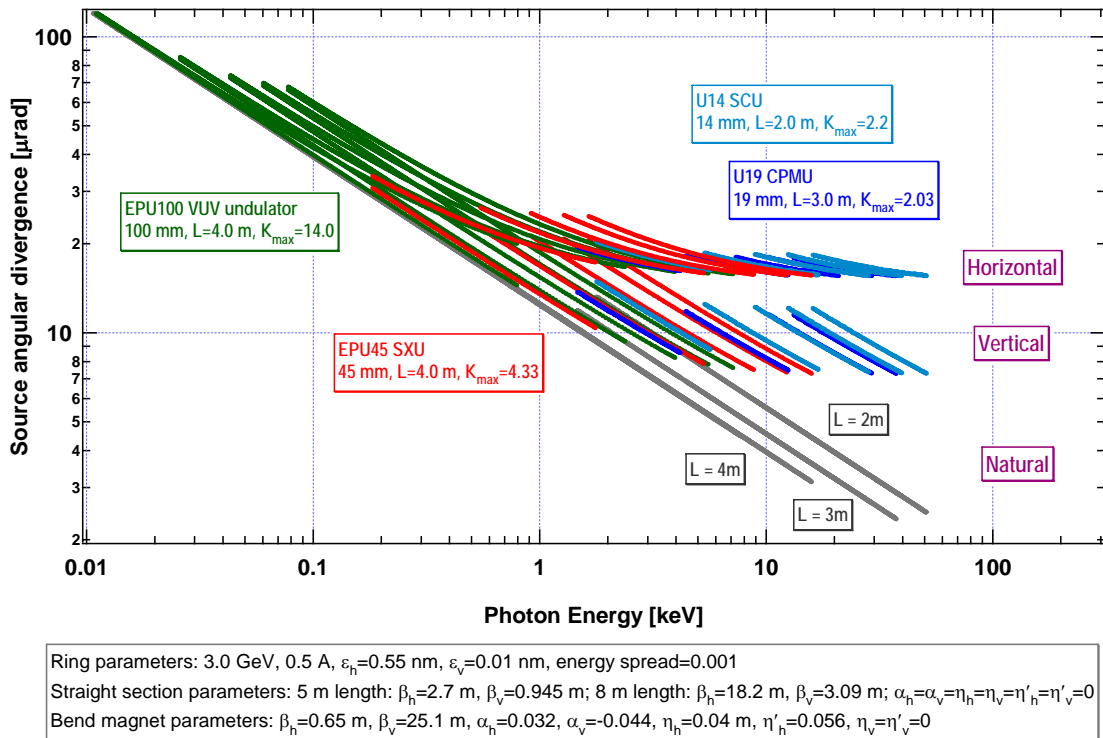


Figure 2.2 : Source Angular Divergence vs Photon Energy

3. Stability Requirements for NSLS-II Beamlines

The experimental programs that will be represented at NSLS-II beamlines have a range of stability requirements. These are elaborated on in the sections which follow. In the table presented here, we summarize the most stringent of these requirements, for each of the major programs, in terms of the beam position stability requirement and the beam angle stability requirement, in both the horizontal and vertical directions. We find, interestingly, that some of the more conventional experimental programs have demanding requirements, in order to satisfy their state-of-the-art science objectives for a cutting-edge source like NSLS-II. We also find that beam position and angle motions could not only have impact on the definitions of the resolution functions (for position, angle, and wavelength) which the beamline optical systems deliver, but also on the intensity throughput which is just as important, for many of these programs, to keep stable. These issues are treated individually for each program. Finally, for some programs, the table below identifies the stability requirements as being in need of further study. It's already clear, for some of these, that the requirements have to be very stringent (e.g. for inelastic x-ray scattering in the vertical direction), but further investigation is needed to determine them in detail, as for example there may be coupling of beam position with beam angle insofar as how they impact the performance of the beamline optical system (which is the case for inelastic x-ray scattering optics).

Program	Vertical Position Stability Requirement (μm)	Vertical Angle Stability Requirement (μrad)	Horizontal Position Stability Requirement (μm)	Horizontal Angle Stability Requirement (μrad)	Radiation Source(s)
Inelastic x-ray scat	Needs further study	Needs further study	Needs further study	Needs further study	CPMU or SCU
Infrared	1	3	2	6	Dipole
Macromolecular cryst	1	1	1	4	CPMU or SCU
Nano-focusing/probe	10% of beam size	10% of opening an	10% of beam size	10% of opening an	CPMU or SCU
Powder diffraction	10	1	10	---	DW or 3PW
Small angle x-ray scat	20	8	8	3	CPMU or SCU
Soft x-ray	10% of beam size	10% of opening an	10% of beam size	10% of opening an	Undulator/dip
High-energy x-rays	50	10	50	---	SCW
X-ray absorption spec	10% of beam size	1	---	---	DW or 3PW
X-ray magnetic circ di	Needs further study	Needs further study	Needs further study	Needs further study	EPU
X-ray photon correl sp	Needs further study	Needs further study	Needs further study	Needs further study	CPMU or SCU

3.1. Stability Requirements for Inelastic X-Ray Scattering Beamlines

All of the concepts which have been investigated for delivering very fine energy resolution x-ray beams involve the use of multiple Bragg reflection crystal optics, often involving asymmetric Bragg reflections and sometimes utilizing back-reflection. These features are all in the makeup of schemes which have been studied already, or are under active investigation, whose objective is to deliver 0.1 meV energy resolution. These have in common that a very narrow vertical angular fan of the beam emerging from the source is employed. For an instrument which delivers 0.1 meV energy resolution, the peak of the spectral distribution function after monochromator needs to be stable to better than 0.01 meV. It is estimated that this would require stability of the incident beam direction (beam angle) to better than 0.04 μrad , i.e. 40 nrad.

The vertical beam position stability can also bear upon this, if the monochromator has a very narrow acceptance aperture. A $0.04 \mu\text{rad}$ shift in angle is equivalent to a $1.2 \mu\text{m}$ shift in position at a distance of 30 m, which is a possible separation between the source and monochromator. In the horizontal direction, the requirements are not nearly as stringent. Because of the coupling of source position and angle motions with their impact on the performance of a high energy resolution device for inelastic x-ray scattering, not to mention the impact on the intensity delivered by such a device, it is suggested that further study is warranted.

3.2 Infrared

Motion of the beam or optical components, whether position or angle, affects the signal reaching the detector at the endstation of an infrared beamline. Typical focal lengths for collecting and transporting beam are on the order of 1 meter, so a $1 \mu\text{m}$ shift in position is equivalent to a $1 \mu\text{rad}$ angular displacement. In general, the optical systems are somewhat more tolerant to angular deviations so for simplicity we state requirements only for position.

We note that some near- and mid-infrared detectors are highly sensitive and would be affected by extremely small beam displacements. However, only a few measurements might exploit this sensitivity, so our stability requirements are based on calculated S/N tolerances as well as practical experience.

Practical experience at the NSLS VUV ring suggests that a 10-fold reduction in beam motion would be beneficial for nearly all measurements, and a 100-fold improvement would reduce noise to a level where its contribution is comparable to other typical noise sources. Measurements of the apparent beam motion at an NSLS IR endstation show displacements up to $50 \mu\text{m}$ when measured at a 1 meter focus (i.e., $50 \mu\text{rad}$). This defines a stability goal of $0.5 \mu\text{m}$ (100X improvement).

Similarly, spectrometer digitizers can resolve to better than 1 part in 10^4 , suggesting a S/N goal of at least 1000:1. This sets a limit on beam position fluctuations at 0.013% of the RMS effective beam size under worst case conditions (asymmetrically aligned Gaussian beam). The effective source size at the shortest wavelength of interest ($2 \mu\text{m}$) is about $200 \mu\text{m}$, defining an absolute goal/requirement of $0.3 \mu\text{m}$ stability. This value is comparable to that estimated from practical experience, so we use this value ($0.3 \mu\text{m}$) as our stability goal.

Though beam motion at any frequency degrades the effective brightness, infrared measurements are directly sensitive to beam motion from a few Hz up to 20 kHz. The $0.3 \mu\text{m}$ stability goal applies to this entire frequency range.

Noise studies at the NSLS VUV ring suggest a mixture of electrical and mechanical sources. Mechanical noise (fans, water pumps) dominates at frequencies immediately below 60 Hz. Electrical noise includes 60 Hz and harmonics (power supplies for magnets) and higher harmonics to a few kHz (phase noise from RF system electronics).

3.3 Macromolecular Crystallography

Mostly as a result of sample size, and the emerging preference to deliver very small beams to the experiment, a position stability of $\sim 1 \mu\text{m}$ or better (horizontally and vertically), at the sample, is needed, and in any case not more than 5% of the sample size which might be smaller than $50 \mu\text{m}$. Note that this translates directly into source stability if the beamline optics focus at 1:1 magnification. As far as angular stability is concerned, it should be within 5% of a sample's rocking curve (which might be as narrow as $\sim 100 \mu\text{rad}$ wide) in the vertical direction, as well as within 5% of the angular separation between adjacent Bragg reflections that need to be distinguished (this separation can be $\sim 1 \text{ mrad}$) in the horizontal and vertical directions. But because the beam-defining aperture, before the monochromator, subtends 50 (80) μrad in the vertical (horizontal) direction, and because the intensity delivered through this aperture must be stable to within 5% or less (see below), these requirements in composite argue for an angular stability of $\sim 2 \mu\text{rad}$ vertically and $\sim 4 \mu\text{rad}$ horizontally. Closer inspection shows that, for the purpose of wavelength stability as required for high-resolution anomalous diffraction measurements, an angular stability in the vertical direction of $\sim 1 \mu\text{rad}$ in the beamline is called for. This is needed in order to preserve the wavelength definition, using a Si(111) monochromator, to within 4% of the width of the very sharp selenium K edge, where measurements are often made. Strictly speaking, this criterion may be relaxed because a beam defining aperture is used before the monochromator, however an angular instability in this circumstance will become an intensity instability. The intensity delivered to the sample should not vary by more than 5% from frame to frame (which might have an exposure time of a few milliseconds), and preferably within 1%, through the entire duration of a full data set from a sample (which might last for as much as one hour). For experiments performed at these beamlines, it is of utmost importance that the final beam conditioning components (apertures and perhaps a final focusing element) be mounted on the same support as the diffractometer holding the sample. For micro-diffraction applications in particular, the total distance spanning these components may be as little as several centimeters. Instruments that meet these needs either already exist or are under active development, and no particular R&D is envisioned to be necessary, in the NSLS-II project, to realize them.

3.4 Nano-Focusing

From the point of view of nano-focusing, a 10% criterion on the position of the beam seems to be an effective stability criterion. A 10% positional instability contributes negligibly to the broadening of the effective spot size. One can imagine that typical images will be generated that will take 1 hour or so. Images that take 10 hours to generate will be considered as experiments that cannot be done, and so eventually all the experiments that will be considered doable will have scans that take at most 1 or 2 hours. Within such a scan it will be important to keep the beam stable to 10%. Typically then after a scan, calibration markers can be used to relocate the beam, and then for the next scan one has to assume that the beam is stable. The maximum overhead one can allow for checking on the beam position is 10% of the typical scan time so that would be of order 10 minutes.

A 10% beam positional stability also translates into less than 1% fluctuations in signal intensity, and this is also acceptable.

3.5 Powder Diffraction

Powder diffraction will probably operate in two modes, area detector and crystal analyzer. The crystal analyzer mode is the most demanding in terms of angular stability, since it aims to provide high d-spacing resolution and precision. Area detector mode is primarily affected by position stability. Both are sensitive to beam energy changes.

In crystal analyzer mode, the critical thing is angular stability. A typical powder peak width using an analyzer crystal is in the range $0.001 - 0.01^\circ$ at 17 keV, depending on the sample quality. 0.001° is unusually good. Let us take 0.005° as typical. Then the beam stability should be 10% of that, i.e. 0.0005° , or $8 \mu\text{rad}$.

A related concern is the energy stability, since energy maps directly to d-spacing in a diffraction experiment. Using Si(111), its intrinsic energy resolution is $\sim 10^{-4}$, which sets a limit on what we can achieve with a sample. If we assume we can find centroids to a few percent of that, we end up with an energy stability requirement of at least 10^{-5} . This maps to an angular stability of 1 or $2 \mu\text{rad}$ (Si(111) at 17 keV has a Darwin width of $15 \mu\text{rad}$), and a monochromator temperature stability of better than 10 K.

All of the above arguments are directed at the plane of diffraction, i.e. vertical.

Area detector measurements are typically 10 times or more lower resolution than this, so are not the limiting case for angular stability. In contrast to the crystal analyzer mode, position stability is important, since position is used as an angle analog. If we assume a focused beamline with a focal spot of $100 \mu\text{m}$ and a detector with similar spatial resolution, then using the 10% rule, beam position stability should be at the $10 \mu\text{m}$ level. Similar arguments apply to the energy stability.

In this case, the spatial stability requirements are in both horizontal and vertical directions.

3.6 Small Angle X-ray Scattering

1. SAXS and USAXS on bulk samples: beam intensity (time) stability

For many small angle x-ray scattering (SAXS) measurements, beam intensity stability is important since the scattering patterns from the sample itself and the sample holder that contributes to the background scattering are measured separately. Since the background scattering sometimes is comparable in magnitude as sample scattering, high beam intensity stability ($<1\%$) is desirable for the purpose of accurate background subtraction. Positional stability is usually not a concern for these measurements.

In a SAXS instrument, the beam size and direction are often defined by apertures that are comparable to or smaller than the full size of the x-ray beam itself. For instance, in the

U(ltra)SAXS configuration, the apertures are 0.1 mm x 0.1 mm and 5 m apart. In comparison, the x-ray beam size at these apertures is likely to be $\sim 95\mu\text{m} \times 30\mu\text{m}$, assuming 0.5 μrad slope error for the KB focusing mirrors. Positional and directional deviation of the x-ray source therefore may result in fluctuations in beam intensity. It can be shown that, in the horizontal direction (aperture size \sim FWHM beam size), the combined motion of the beam at the beam-defining aperture must be less than 8% of the beam size, or 8 μm , in order to satisfy the 1% intensity stability requirement; whereas in the vertical direction, the allowed beam drift is more than 20 μm . These requirements are 17 μm and 54 μm , respectively, if 5% beam intensity stability is desired. The requirements are much less stringent when the aperture size is relaxed or if the beam size is improved with better focusing optics. The proposed 10% source position (4 μm) and direction (2 μrad , 2.5 m arm, 5 μm) instability each can satisfy the most stringent requirement of $<8 \mu\text{m}$ horizontal beam drift.

2. Micro-beam SAXS: position and intensity stability

In this configuration, with a target spot size at the sample of a few μm , the beam is first focused onto an aperture that defines a secondary source (there could also be two separate secondary sources for horizontal and vertical focusing) for the micro-focusing mirrors. The beam at the sample can therefore have very good position stability but its intensity will be determined by the amount of x-ray beam that passes through this aperture, which in turn depends on the positional stability of the source. The size of this secondary source, dictated by the combined requirements of low beam divergence ($\sim 0.8 \text{ mrad}$) needed for the purpose of SAXS measurements and small spot size (1 μm), is $\sim 19 \mu\text{m}$ (horizontal, at 45 m, 2:1 focusing for primary KB) by 6.5 μm (vertical, at 57.5 m, $\sim 1:1$ focusing for primary KB). Note that due to the slope error of the primary focusing mirror, the image of the source (25 μm (H) and 28 μm (V)) will be much larger than the size of the aperture that defines the secondary source. The proposed 10% maximal source position drift therefore will result in $\sim 1.7\%$ (horizontal, 2 μm) and $\sim 0.05\%$ (0.4 μm) change in flux that pass through the secondary source-defining apertures, which is close to the desired 1% beam intensity stability at the sample.

3.7 Soft X-Ray

The monochromator designs for the initial soft x-ray beamlines at NSLS-II are envisaged to be some sort of variable line spacing, collimated plane grating monochromator (VLS-CPGM). Design variations for ultra-high resolution mode (3600 l/mm) and high flux mode (300 l/mm) were evaluated for the CDR. For those gratings, the expected energy resolution of the beamlines is:

3600 l/mm:	11 meV @ $h\nu = 1000 \text{ eV}$, 2 meV @ $h\nu = 200 \text{ eV}$
300 l/mm:	114 meV @ $h\nu = 1000 \text{ eV}$, 21 meV @ $h\nu = 200 \text{ eV}$

The main effect of motion in the vertical direction is to produce a degradation of the energy resolution. However, the energy shift of even a very large beam motion of 4 μm in the vertical direction is almost negligible:

3600 l/mm: 0.89 meV @ $h\nu = 1000 \text{ eV}$, 0.08 meV @ $h\nu = 200 \text{ eV}$
300 l/mm: 11 meV @ $h\nu = 1000 \text{ eV}$, 1.0 meV @ $h\nu = 200 \text{ eV}$

For motion in the horizontal direction, the main impact will be to shift the image at the focus of the last pair of refocus mirrors. However, the demagnification in the horizontal direction is over 50:1. Therefore, even a 10% shift in the source point will produce only a 0.2% shift in the position of the focussed beam.

With regard to stability of the angle of the photon beam, again a 10% criterion will more than satisfy experimental concerns. At that level, the fractional change in the wavevector of the photon beam is about 1 part in 10^{12} in the horizontal direction and 1 part in 10^{14} in the vertical direction.

3.8 Superconducting Wiggler Beamlines

Superconducting wigglers can be used as photon sources for angular dispersive x-ray diffraction (ADXD), energy-dispersive x-ray diffraction (EDXD), x-ray imaging and radiation therapy research.

For ADXD of large (approximately 1 mm) samples, x-rays are typically focused by a sagittal focusing monochromator at a magnification of approximately unity. A position stability of 10% of sample size results in a source-position stability of approximately 100 μm horizontally and vertically. For ADXD of small samples of a few μm in diamond anvil cells, K-B mirrors (at a magnification of approximately 100:1) are typically used to focus the x-rays. A position stability of 1 μm at the sample requires a source position stability of 100 μm horizontally and vertically. In both cases, wavelength stability of 10^{-4} and usage of a silicon monochromator at a Bragg angle of approximately 0.1 rad require the vertical angular stability to be within 10 μrad .

EDXD experiments that require the most orbit stability are those that use the peak position as a figure-of-merit. These include strain mapping and deformation experiments. For such experiments, the angle of the incident beam is defined by a fixed slit and the source, with the diffraction angle (2θ) typically being 0.1 rad. To obtain 10 micro-strains ($10^{-5} \Delta d/d$) accuracy, the incident angle as defined by the slit and source should be maintained to within $10^{-6} \mu\text{rad}$. The source and beam-defining slit being 50 meters apart, the vertical source position should have a stability of 50×10^{-6} meters, or 50 μm .

For imaging (DEI and micro-CT) and micro-beam radiation therapy (MRT) experiments, the distance between the subject and detector is typically 1 meter, and a resolution of $\sim 1 \mu\text{m}$ is typically desirable. Assuming a 50 meters source-to-subject distance, the source position should be stable to within 50 μm horizontally and vertically.

To summarize, for typical superconducting wiggler applications, the source position should be stable within 50 μm horizontally and vertically, and the source vertical angle should be stable within about 10 μrad . There is no requirement on source horizontal angle due to the large horizontal divergence afforded by a superconducting wiggler.

3.9 Timing Experiments

NSLS II is expected to serve a number of time-resolved measurement techniques having resolution of ~ 1 ps. This defines a requirement for the phase stability of electron bunches.

Some time-resolved techniques are based on synchronized, ultra-fast lasers. The frequency response of their synchronization systems is highest at low frequencies, becoming less effective above ~ 250 Hz (response of PZT transducers). So electron bunch phase stability is less critical at low frequencies.

3.10 X-ray Absorption Spectroscopy

Fluctuations in intensity, unless extreme, are handled by normalization. As integration times are generally one to several seconds per data point, x-ray absorption spectroscopy (XAS) is less sensitive to high-frequency instability. Beam position at the sample is a function of source position and angle, and of beamline optics as energy is scanned over a typical 1000 eV. While classic EXAFS samples are perfectly uniform over several mm and thus insensitive to beam position, cutting-edge XAS often involves highly inhomogeneous materials. These require beam position stability of 5-10 μm at the sample (the finest scale of heterogeneity likely to be significant for bulk measurements) over several energy scans. Energy stability is a function of source angular stability and the thermal and mechanical stability of the monochromator. For high-resolution applications, such as phosphorus, chromium, manganese and arsenic K edges and several important L and M edges, spectral features used to differentiate chemical species may differ by as little as 0.1-0.3 eV. Energy stability should then be within 0.05 to 0.1 eV for the duration of an experiment. Source position is generally less of a consideration for bulk XAS, as stability is expected to be within $\sim 10\%$ of source size. Angle of the source beam is more critical, as it influences monochromator energy selection and beam position projected through optics to the sample. For energy stability of 0.05-0.1 eV, a source vertical angle stability of ~ 1 μrad is needed. For position stability, angular deviation can be ameliorated through use of apertures close to the sample, provided the apertures are over-filled by at least the projected position deviation, and this is small relative to the beam size. In contrast, horizontal stability requirements are less rigorous, as the source size and divergence are greater and by nature less of the horizontal extent of generated beam is used. Considerations of stability are compounded by the potential variety of beamline optical components (which can amplify or create instability) and source types (soft bend, hard-bend equivalent, damping wiggler). For vibrational stability, it is expected that final apertures and intensity measurement will be mounted monolithically with the sample stage and detectors. Upstream optics (monochromator, apertures, focusing elements) should be similarly grouped. An active vertical feedback system (as successfully implemented at NSLS X15B) may be necessary to achieve the required stability. While current instrumentation and technology exists for high-resolution monochromator and feedback systems, it is expected that some R&D will be required to combine these aspects for XAS applications at NSLS-II.

3.11 X-ray Magnetic Circular Dichroism using Fast Switching Circularly Polarized Soft X-Rays

For x-ray magnetic circular dichroism (XMCD), the polarization profile of the photon beam is of importance. Changes in the position of the electron beam may or may not influence the polarization ratio between the left and right circularly polarized soft x-rays.

A more extensive study needs to be done to quantify the variations in the polarization ratio, if any, and the impact that this will have in experiments. As an estimate to what is currently possible in sensitivity, currently at X13A we are able to measure the difference signal (in form of hysteresis loops) smaller than 2×10^{-5} . This signal corresponds to the nitrogen hysteresis loops recorded on iron nitrates where the nitrogen is hybridized with the iron.

We will study the case of a beamline with 2 x 2 meters EPU's for NSLS-II for fast switching circularly polarized soft x-rays. Movements in the electron beam in angle across the straight section will not affect too much the polarization ratio if the undulators are completely symmetric respect to the center of the straight section. The polarization ratio will present problems combining shifts and angle movements. In that case the angle will not be centered and different sections of the polarization profile for each insertion device will be extracted. The effect will depend on the polarization profile of each photon beam (how much the polarization changes from the central cone to the extremes of the distribution) and the shift either in horizontal or vertical.

Impact of:	on:	Polarization Ratio	Beam Overlap	Photon Energy
Horizontal shift		no	no	no
Vertical shift		no	no	no
Horizontal angle		no	yes?	no
Vertical angle		no	yes?	yes
Shift and angle		yes	yes?	yes

4. Conventional Construction

The role of conventional facilities in assuring beam stability goals for NSLS II is driven by two primary objectives: (1) providing a structural platform that meets vibration criteria and (2) providing an environment that meets temperature stability criteria. Of these two objectives, the most challenging is assuring that the storage ring tunnel floor and the experimental floor are sufficiently stable to ultimately achieve focused x-ray beam resolution of 1 nm or better.

The source of vibrations affecting NSLS II are pre-existing or cultural vibrations related to the selected site, vibrations due to the machine itself and vibrations generated by the supporting facilities. Cultural vibrations are a function of the geologic conditions transmitting vibration to the site and proximity to surrounding sources such as road traffic and machinery in adjacent facilities. Vibration sources due to the machine include the flow of cooling water through devices, the physical support systems and electromagnetic forces. Vibration sources associated with supporting facilities include power, cooling, HVAC and foot traffic associated with operation of the light source buildings and ancillary systems. Facility vibration sources and to a lesser extent, cultural vibration sources, are heavily influenced by the layout, structural and mechanical design of the light source facility and its support systems within the scope of conventional facilities.

Ground motion at the NSLS-II site has a complex spectrum consisting of fast and slow motion. Slow motion characterized by long wavelengths is the result of ocean swells, wave action and crustal resonances (a few Hz depending on the structure of the subsurface). Waves arriving at the site with wavelengths larger than the diameter of the NSLS II will not affect the stability of the beam. Cultural noise on the other hand with frequencies higher than a few Hz has the potential of dramatically affecting its performance through the coupling that exists between lattice movement and beam distortion or jitter especially when the motion is uncorrelated. In order to achieve the desired stability in the accelerator beam, the uncorrelated band of cultural noise must be kept at a minimum since it is the dominant source of beam jitter.

While the first line of defense is the selection of a quiet site characterized by reduced levels of vibration throughout the uncorrelated frequency band and especially the band segment within which the fundamental frequencies of systems supporting the lattice magnetic elements are found, that alone does not suffice. Cultural noise within the critical frequency band generated by accelerator-related systems will inevitably be generated and travel around the facility. Therefore the role of the structure (its design as well as its interface with the supporting medium) is critical.

At sites, where the building foundation is coupled to bedrock (a rock site), with an accelerator foundation of any thickness, the floor will assume the vibration levels of the free-field. In the case of foundations supported on sand/gravel (a soft site) such as NSLS-II, the foundation will alter the free-field motions by filtering out a wavelength band associated with the dimensions of the structure. Rock sites, on the other hand, are more susceptible to cultural noise generated by operating equipment in the vicinity of the

structure than soft ground counterparts. Therefore, determining in advance, the specific interaction between the foundation structure and the free-field environment as well as the anticipated induced vibrations is essential for design of sensitive facilities. The stability of the operation at levels demanded by the next generation light sources like the NSLS-II can only be met through a fully coupled, complimentary relationship between the performance goals driving the accelerator stability requirements, the NSLS II site ground motion environment and the design of the structural elements of the accelerator.

Discussed below are (a) the NSLS-II site and its established ground vibration environment under green-field conditions including comparison with vibration stability experience from operating 3rd generation light sources, (b) quantification of ground motion criteria for the accelerator ring and the experimental floor, (c) an overview of the on-going studies aiming to arrive at design features that will help keep the uncorrelated motion at a minimum thus ensuring stability of the beam, and (d) a list of R&D activities to be pursued that will help in understanding the relationships between ground motion and beam jitter as well as exploration of noise suppression techniques or structural design features.

4.1 NSLS-II Site and Ground Motion Environment

Geophysical studies conducted at the BNL site over a number of years suggest that the NSLS II will be built on generally uniform, well-settled glacial sands forming a well-characterized 1400-foot layer above the bedrock. The water table, which is an important feature to be considered in establishing the ground motion environment including its frequency content, is situated at approximately 30 feet below grade (~ 10m). The shear wave velocity in the upper strata of the subsurface has been estimated to be 886 ft/sec. Given that the coherence in ground vibration, which in turn is affected by the variability in geologic conditions at any given site, is a very important parameter in ensuring that the spatial variation of motion in a sensitive facility is kept at a minimum, the homogeneity exhibited by the NSLS II subsurface will help minimize spatial variability in ring floor motion.

In general, a rock site has some advantages for a sensitive facility such as the NSLS-II due to the significant reduction of cultural ground motion that occurs as a result of the absence of surface layer made of much softer material which can trap or amplify waves propagating through it. On the other hand, a homogeneous, well-settled sandy subsurface has properties that are superior to those of a rock site in terms of filtering ground motion arriving at the site as a result of foundation/soil interaction and arrest of facility-generated noise from operating systems. The impedance difference between the accelerator foundation and the subsurface it is laying on, which is higher in the case of a sandy subsurface, plays a key role in reducing ground vibration on the ring or the experimental floor due to vibration from rotating machines on a near-by but separate foundation. In the case of a hard rock site, however, the impedance difference between the supporting ground and the facility floor is minimized, allowing the rock to act as a conduit of noise generated in the nearby facilities.

To assess the ground vibration that exists at the NSLS-II site under “green-field” conditions, field studies have been performed and results were compared with free-field conditions that exist in other facilities. Figure 4.1 depicts power spectral densities of vertical motions both measured recently at the NSLS-II site and two key locations at Spring-8 facility which represents the quietest of all the light source sites. Also listed is integrated rms vertical displacements for the frequency range of 2-100 Hz. The two measurements at the Spring-8 free-field at a location of rock outcrop outside the ring perimeter exhibit vertical displacements of 2-3nm while the third measurement made on the surface of a soil layer~ overlaying the Spring-8 rock and near the long experimental line end-station exhibits vertical rms displacements higher than those measured at the NSLS-II site (~20 nm). Figure 4.2 represents measurements performed near the NSLS-II site with similar subsurface conditions and which demonstrate the positive role played by the foundation mat of the CFN facility in reducing the vibration that exists in the free-field.

4.2 NSLS-II Storage Ring and Experimental Beamline Stability Requirements

The requirements for the NSLS II storage ring floor stability stem from the uncorrelated part of the ground motion that is expected to reach the floor and propagate around the ring inducing distortions in the relative position of the magnetic elements in the lattice. As mentioned above, ground motion waves reaching the ring floor that are of the order of the betatron wavelength or smaller (~13 m) are the ones that are of concern because of the lack of correlation that they exhibit.

Slow ground motions with wavelengths larger than the characteristic dimensions of the accelerator (i.e. diameter) or with characteristic frequencies below 1 Hz do not have serious effects on the stability of the beam despite the fact that they result in much larger floor displacements because the motion they induce is correlated and can be appropriately corrected. For example, ocean wave action with characteristic frequency of about 0.2 Hz and a surface wave wavelength of ~1,200 m (~4,000 feet) is expected to have space and time coherence. Correlation studies have also shown that the “slow” band of the fast motion or cultural noise (band between 1 and 4 Hz) is highly correlated and therefore can be easily corrected. Thus, it is the incoherent nature of the fast motion (mostly cultural noise) reaching the ring floor and exhibiting characteristic frequencies higher than a few Hz (> 4 Hz) that will induce distortions in the beam. As a result, the integrated displacement for the range of interest (range that encompasses the fundamental frequencies of lattice magnet systems supported on the ring floor and expected to amplify the floor motion) must be kept as low as possible. Based on relations that link ground motion with beam jitter (i.e. establishment of response functions between the movement of a lattice magnetic element and jitter on the beam) while taking into account anticipated vertical motion amplification between the ring floor and the magnetic element reference, the upper limit of the tolerated rms vertical displacement at the ring floor level and for the range between 4-50 Hz has been set at **25nm**.

The sources are the external (natural/cultural) and the self-generated. To ensure that the vibration criteria for stability are met design features must be implemented that maximize

attenuation of cultural as well as self-generated vibration sources. These design features include optimization of floor thickness, monolithic structure with the experimental floor, isolation from the operating mechanical systems and selection of well balanced machinery.

The ground vibration measurements at the NSLS-II site (~20 nm in 2-10 Hz) aided also by the expected filtering (shown in the case of CFN) due to the interaction of the NSLS-II floor structure with the supporting soil, indicate that the requirement of maintaining the uncorrelated vertical displacement (< 25nm for the 4-50 Hz range) is achievable. Recent vibration studies conducted on the experimental floor and the storage ring foundation of the APS which is subject to similar geologic and cultural noise conditions indicate that the two important criteria namely the 25 nm rms vertical ring floor displacement and the minimization of the differential movement between locations on the experimental floor to an order of 1 nm or less can be realized, with the latter requiring special design of the experimental floor section supporting extremely sensitive beam lines.

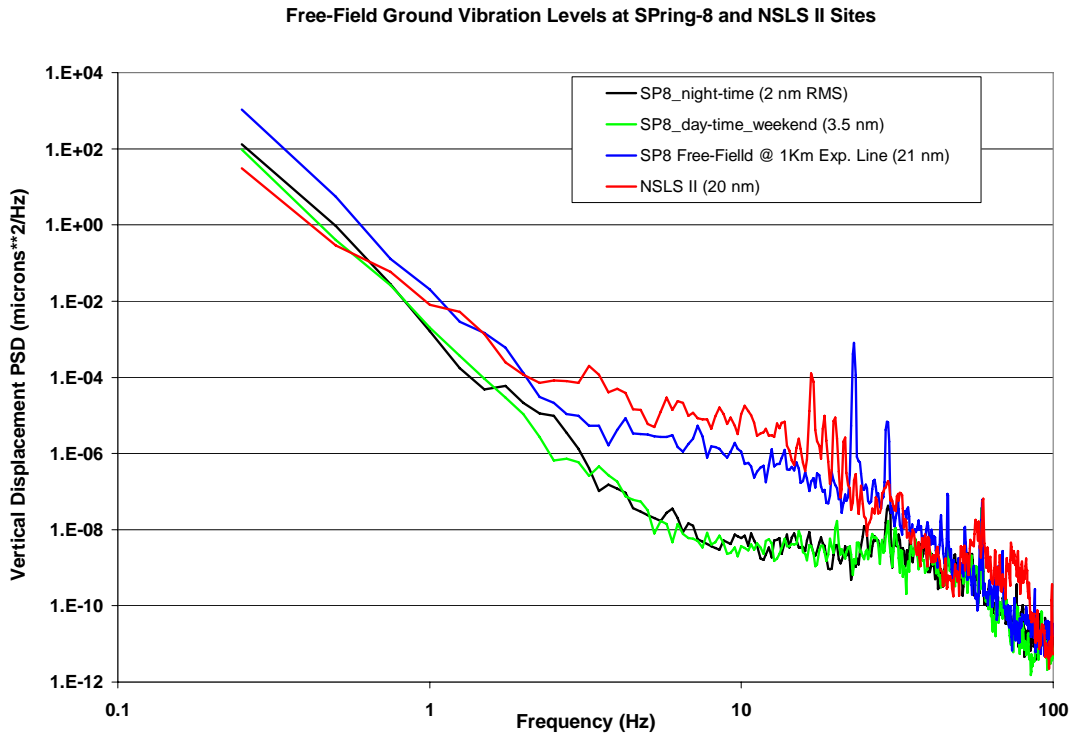


Figure 4.1: Vertical displacement PSD measured at the NSLS II site and at the SPring-8 facility

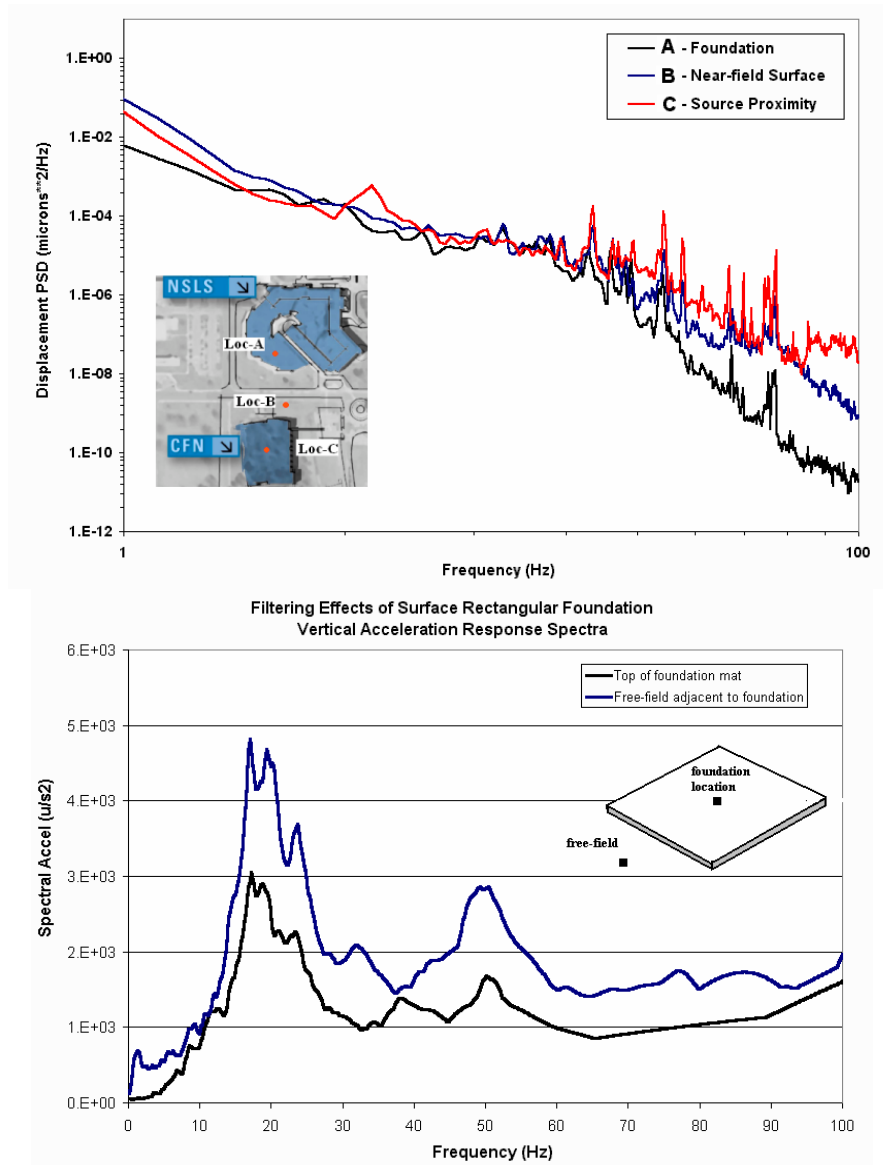


Figure 4.2: Filtering of the free-field ground motion measured at the CFN floor. Fig. 4.2a depicts the attenuation path of the cultural noise generated at the NSLS facility. Fig 4.2b shows the reduction in the ground motion response spectra of the CFN near-field and the CFN floor.

While the overall requirements for stability of the experimental lines having their infrastructure supported on the experimental floor mat are inevitably coupled and driven-by requirements established for the ring, there are special requirements needed to be met on the experimental floor in order to satisfy the variety of sensitivities that characterize experiments at the end stations. This stems, primarily, from the 1nm X-ray optics desired by some of the experimental lines. From the structural point of view, the desired criteria for both the ring and the experimental lines can be met with careful consideration of (a)

the ground vibration environment at the NSLS-II site, (b) implementation of special structural features that maximize the filtering of ground motion and minimize the differential movement between the ring and the experimental floor, and (c) designing the experimental station support infrastructure in close relation to the floor motion amplification characteristics and thus minimizing differential movements between the reference beam position and the imaging point.

The stability requirements on the NSLS-II experimental floor can be separated into two groups, specifically, the 1nm-level sensitivity lines and experimental lines such as infrared that desire beam motion limits below $0.25\mu\text{m}$. The stability of either group is inherently linked to the electron beam stability whose jitter is a function of the movement of the ring floor. Taking into consideration that ground motion can be divided into “fast” and “slow” regimes (fast being the motion above a few Hz and assuming increased incoherence time and space incoherence with increased frequency) a desired upper limit of vertical ring floor displacement (rms) has been set at 25nm for the fast motion covering the range between 4 and 50 Hz. It should be pointed out that due to structural differences between the NSLS II ring and the experimental floor (ring foundation mat has higher thickness that provides both global rigidity and vibration filtering), the rms vertical displacement on the experimental floor is expected to be higher than its ring counterpart. The temporal and spatial variability that is expected to be seen on the experimental floor (also observed in other operating light sources) will require special care in order to satisfy the requirements of very sensitive experimental lines. Figure 4.3 depicts spatial and temporal variation in measured power spectra density (μ^2/Hz) and the rms vertical displacement at two locations on the Spring-8 experimental floor separated by 90m distance.

To ensure that the vertical differential motions between two locations on the experimental floor supporting the most sensitive experimental lines requiring imaging resolution of the order of 1nm is minimized and can satisfy the stringent requirements, structural enhancements need to be implemented. Specifically, by supporting the last optical element of the 1nm resolution line and the imaging point on the same support structure which is designed with dynamic properties that fall outside the motion amplification regime of the floor motion will ensure that the differential movement of these two key reference points is eliminated. Further, by creating a rigid link between the extraction point and the imaging point (achieved by enhancing the floor mat thickness locally which will provide the rigidity required) the differential motion of distant locations on the experimental floor can be minimized. The motion isolation of experimental floor sections supporting sensitive lines can further be enhanced with special structural features that will help interrupt the propagation of waves traveling on the experimental floor. The synergy between the structural enhancements, the understanding of the floor motion frequency content and amplification characteristics and the active feed-back and correction will ensure that stability which can support the 1nm resolution imaging can be achieved.

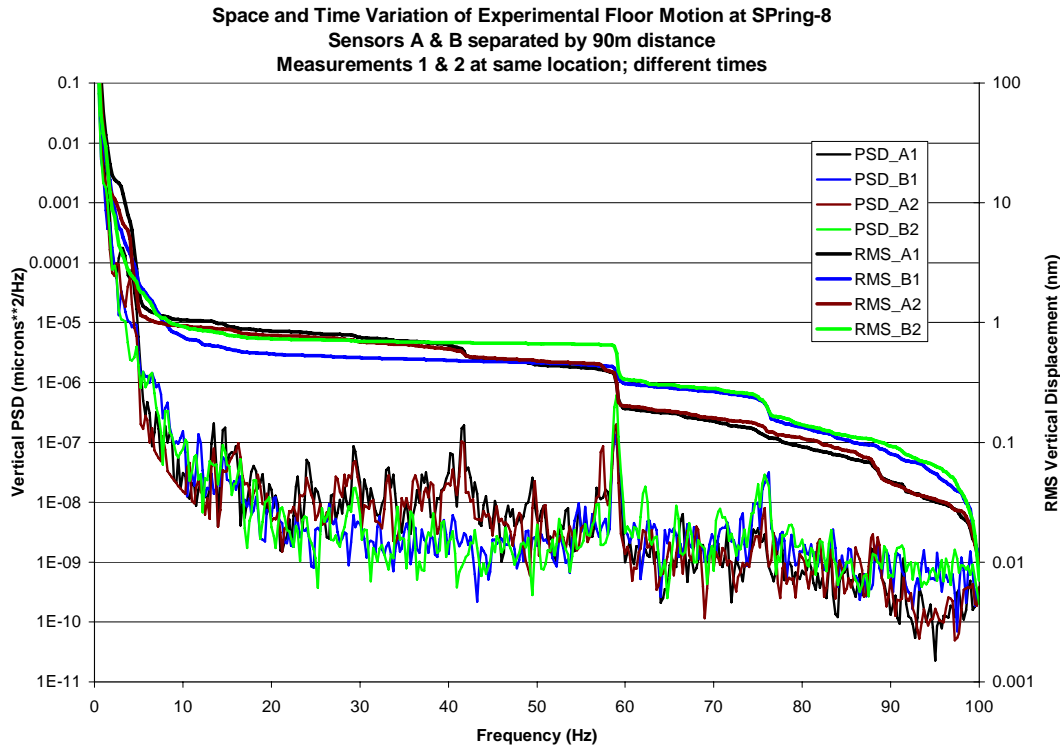


Figure 4.3: Measured displacement power spectral densities and rms displacements on the Spring-8 experimental floor demonstrating both temporal and spatial variability of floor vertical motion

4.3 Structural Considerations

In an effort to predict the vibration characteristics at the ring and experimental floors subject to the existing natural noise environment and the anticipated cultural noise from the NSLS II operating systems, an extensive analysis based on detailed modeling of the site and the structures that are expected to play a role in both the generation of vibration as well as its filtering has been initiated. The primary goals of this comprehensive analysis/simulation of ground motion interacting with the NSLS-II facilities are (a) the optimization of the ring floor thickness while meeting the set criteria for vertical rms motion, (b) estimation of the contribution of NSLS-II system-generated noise towards the threshold criteria and the identification of the optimal configuration that interferes in the propagation of self-generated noise including structure-to-structure interaction, (c) assessment of special noise path interruption features that will help minimize cultural noise traveling on the experimental floor towards extremely sensitive lines.

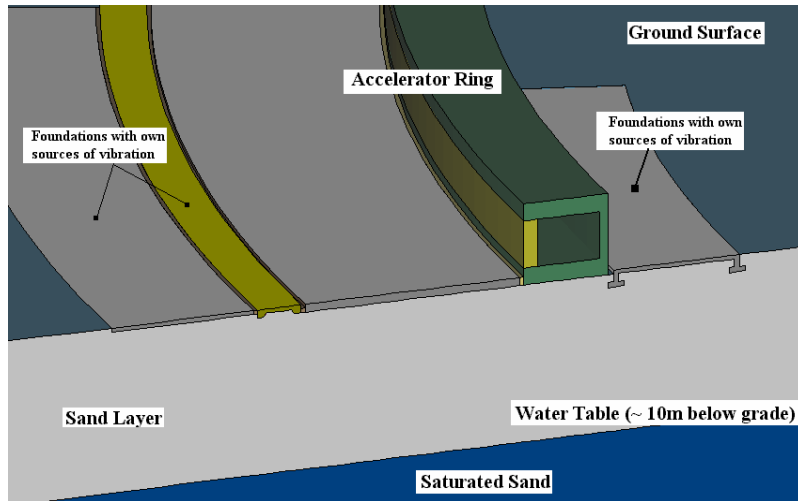


Figure 4.4: Structural details of the interfaces between the NSLS II ring, the experimental floor and the service buildings (baseline)

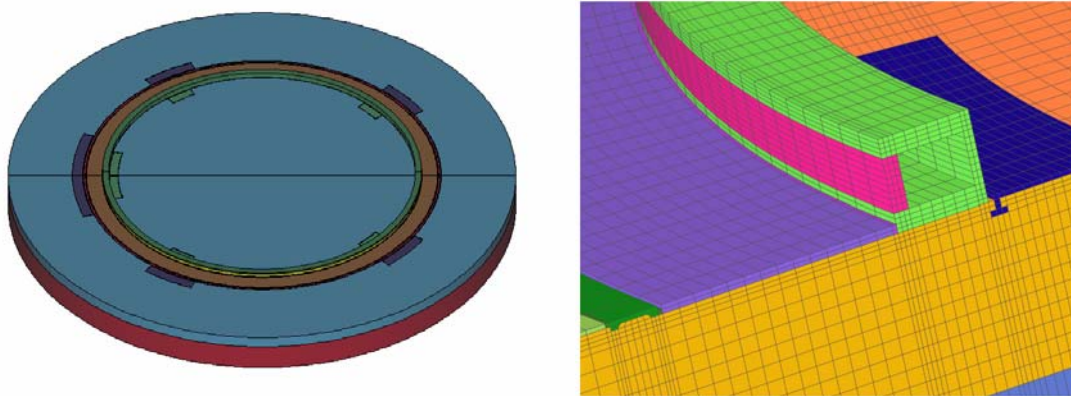


Figure 4.5: Comprehensive model generated to study the interaction of the NSLS II facility with the ground vibration (natural and cultural) at the proposed site

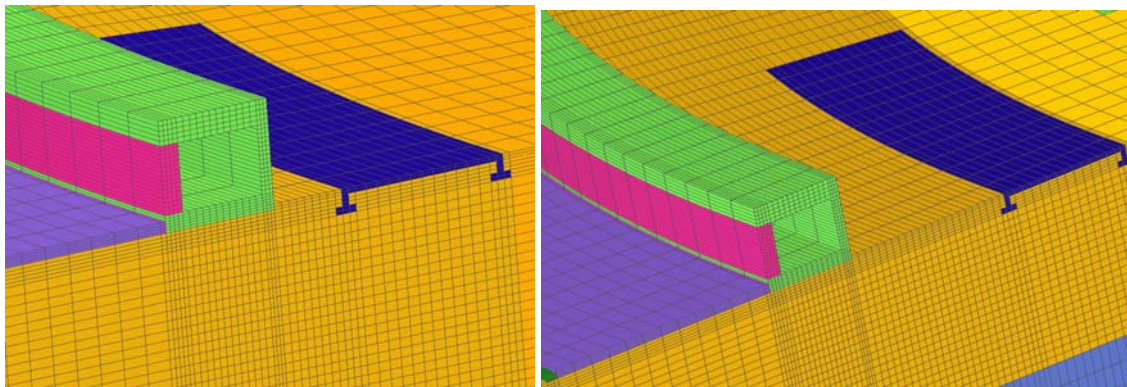


Figure 4.6: Alternative options being explored to enable further minimization of in-house generated cultural noise from facility operations

Figures 4.4 and 4.5 are actual numerical (finite element) representations of the closely coupled structural elements of the NSLS-II accelerator including the supporting surface soil layer and the layer below the water table. Studies to-date focused on the scattering and attenuation characteristics of noise generated on the service building foundation, the access corridor and the free-field. In anticipation that the bulk of the self-induced noise will originate on the service building floor, attenuation options that include, but not restricted to, the increase of distance between the ring floor and these sources are being explored (see Figure 4.6). To help guide the optimization effort, vibration measurements in the proximity of operating mechanical equipment such as chillers and pumps were conducted at other facilities. Results shown in Fig. 4.7 indicate the significant attenuation that occurs even at small distances ($\sim 2\text{m}$) away from the supporting pads. In addition, the effectiveness of special isolation joints was studied at the two facilities (APS and Spring-8) for implementation into the design of the NSLS II service building and experimental floor.

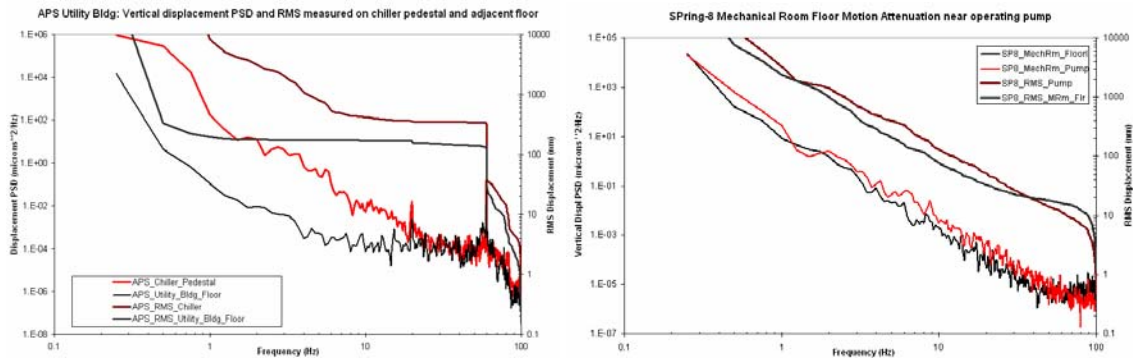


Figure 4.7: Motion attenuation studies on the floors of utility buildings serving the APS and Spring-8 facilities

Based on past experience, actual field measurements at different facilities (including NSLS, APS, Spring-8, CFN, etc.) and the to-date results of the detailed analyses the following structural considerations have been used in guiding the design of a “quiet” facility that will meet the required stability criteria:

- Maintaining a monolithic structure between the ring and the experimental floor to maximize filtering of ground motion present at the site
- Maintaining a structural “box beam” structure for the accelerator tunnel to stiffen the tunnel floor and adjacent experimental floor
- Enhancement of the experimental floor thickness supporting the most sensitive experimental lines to form a “rigid” connection between the beam extraction (reference point) and the focal point at the end of the line leading to the minimization of differential movement
- Minimization of the amplification of motion between the experimental floor and the elevations of interest (reference and focal points) by selecting the dynamic properties of the support structures according to the frequency content of the floor motion (including base isolation) and by mounting the last focal element and the focal point on the same support

- Consideration of arresting noise generated on the experimental floor and propagating towards the sensitive experimental lines by introducing special isolation joints (trenches) that disrupt the movement of motion on the floor acting as a wave guide but do not reduce the overall ring/experimental floor rigidity.
- Implementation of special isolation features between the experimental floor and the outer accelerator structures that are subject to noise generation. Recent field measurements at the APS floor demonstrated the effectiveness of such isolation features

4.4 Thermal Stability

Thermal stability of the storage ring tunnel environment, and to a lesser extent the experimental floor, is required to minimize the effects of thermal expansion/contraction of machine components. This is most critical in the storage ring tunnel where temperature changes can cause deflection of the girder system supporting storage ring components. For this reason, the most demanding temperature stability requirement is to achieve stability of $\pm 0.1^{\circ}\text{C}$ per hour in the tunnel. Temperature stability on the experimental floor is not as critical and can be maintained at $\pm 0.5^{\circ}\text{C}$ per hour or nominally 1°F . There will be applications where more stringent temperature requirements will apply within hatches on the experimental floor. These applications will be addressed within the design of the experimental beam lines.

The ability to achieve thermal stability of $\pm 0.1^{\circ}\text{C}$ within the storage ring tunnel has been demonstrated at other Light Source facilities and other facilities at BNL. The relatively stable nature of the load and heat rejected to the space makes this requirement quite achievable when coupled with well designed HVAC systems that utilize high precision/high resolution instruments and controls and air handling equipment capable of being modulated to achieve precise outlet conditions. BNL has installed similar systems in high accuracy laboratory settings that have achieved stability performance of 0.05°C . Additional modeling of airflow and temperature distribution will be performed to assure these techniques are consistent in the tunnel environment.

The ability to achieve thermal stability of $\pm 0.5^{\circ}\text{C}$ or nominally 1°F on the experimental floor is readily achieved by commercial HVAC systems provided proper attention is placed on selection of industrial grade instrumentation, location of instrumentation, control logic, proper distribution of supply and return airflow and limiting variability of external sources such as direct sunlight, infiltration or poorly insulated surfaces.

Conventional facilities will also provide chilled water and tower water for cooling of process water systems used to cool accelerator components. Temperature control schemes for process cooling water are described in the Mechanical Systems section of this report. Additionally, conventional facilities will provide feedback of the status of key conventional facilities systems parameters to the accelerator control system for monitoring and use in accelerator systems control.

4.5 Envisioned R&D

The necessary R&D must focus on both the floor motion characteristics which are both site-specific as well as structure-specific and the effectiveness of design features that will enable the suppression of floor motion (both absolute and relative). The major efforts should include:

- A detailed study of the ground motion expected to filter through the ring and the experimental floor including its spatial variability, response spectral characteristics as well as correlation properties. This will combine green-field ground motion measurements and global NSLS-II structure interaction.
- Assessment of effectiveness of varied design approaches for structural and mechanical systems at minimizing vibration of the accelerator floor
- Assessment of the effectiveness of experimental floor structural features (i.e. local mat thickness enhancement, trenching, base isolation, etc.) through benchmarked numerical studies that will help guide the design of the sensitive experimental lines.
- Continue to monitor and analyze the NSLS-II site ground motion characteristics including spatial and temporal variation, dedicate R&D in studying site-specific slow ground motion (<0.01 Hz) which, even though has all along been considered to have complete space and time coherence, may be dominated by residual inelastic and non-correlated components that will ultimately have an effect on the beam.
- Utilize thermal dispersion modeling software to verify tunnel temperature stability objectives will be achieved.

5. Mechanical Systems

5.1. Mechanical Stability Requirements

Storage ring girders provide a common mounting platform for the dipoles and multipole magnets including correctors. They also support vacuum chambers on which 7 of the 9 BPM buttons of a cell are flange-mounted. Mechanical stability of the girders, magnets and vacuum chambers are, therefore, critical to providing a stable beam to the users.

Various sources such as ambient floor motion, flow-induced vibrations and thermal transients [Ref.5.1] can affect the mechanical stability of the girder assemblies. Based on the beam stability criterion of 10% of the beam size, tolerance limits for random magnet and girder motions in the vertical and horizontal directions were established as shown in Table 5.1.

Table 5.1. Tolerance Limits on Random Motion

Tolerance Limits	ΔX RMS Quads	ΔY RMS Quads
Random magnet motion	$< 0.15 \mu\text{m}$	$< 0.025 \mu\text{m}$
Random girder motion	$< 0.6 \mu\text{m}$	$< 0.07 \mu\text{m}$

Since the beam size in the vertical direction is significantly smaller than in the horizontal direction, the tolerance requirements in the vertical direction are more stringent. The design and analyses of the magnet-girder-vacuum chamber support system presented in the following sections will focus on the motion in the vertical direction.

5.2. Conceptual Design of the Storage Ring Girder Support System

a) Storage Ring Girders

A conceptual design for a typical girder with its mounting pedestals is shown in Fig.5.1. The nominal length is approximately 3.0 m for the dipole girders and 3.2 to 5.7 m for the multipole girders. The girders are approximately 0.8 m wide and 0.4 m high. They will be fabricated by welding commercially available ASTM A-36 steel plates and channels of thickness ranging from 1 to 2 inches. After welding, the girders will be stress-relieved by vibratory stress-relief equipment.

Since the ambient ground motion decreases sharply as inverse of the fourth power of frequency, the girders are designed to achieve natural frequencies of greater than 50 Hz. To achieve this, eight cross plates of 4-inch width and 2-inch thickness will be provided as stiffeners. The natural frequency of the NSLS-II magnet-girder support system will be further improved by eliminating elaborate alignment mechanisms. Additionally, lowering the beam height to 1m in the tunnel allows for low-profile stiff girders. The girders will be mounted on 2-inch thick steel pedestals that are grouted to the floor with a non-shrinking epoxy grout. For mounting and height adjustment, eight 2-inch diameter bolts with steel washers will be used.

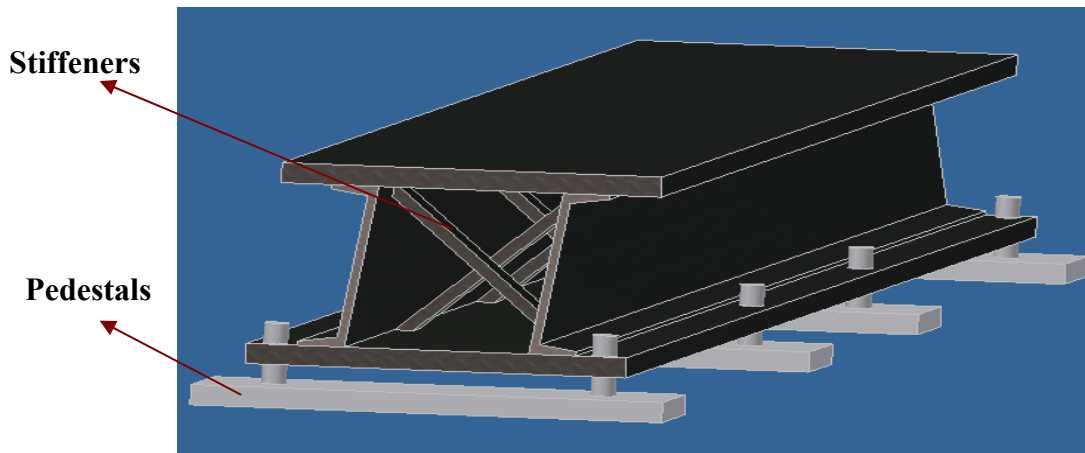


Fig.5.1 Conceptual design of NSLS-II storage ring girder

Based on studies performed at the BNL site, it is expected that the relative settlement of the soil supporting NSLS-II would be $10 \mu\text{m}/10 \text{ m}/\text{year}$. To accommodate this ground settlement in the girder design, the pedestal supports located at the two ends of the girder are designed to be comparatively flexible. This can be achieved by using Belleville washers (Fig. 5.2) which have a spring characteristics of constant force in the mid-deflection range due to their conical shapes.

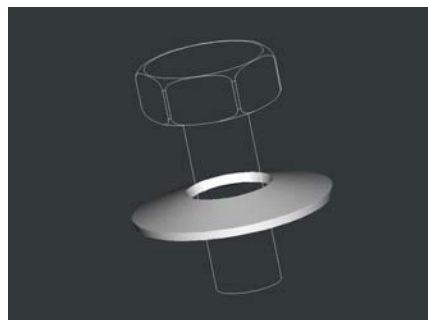


Fig.5.2 A Belleville washer

(b) Vacuum Chamber Supports

Each vacuum chamber will be supported by a relatively stiff support in the middle and two flexible supports at the ends (Fig. 5.3), which would allow the chamber to expand during bake-outs. The BPM buttons will be mounted as close to the fixed support as practical. The chamber supports will be made from Invar 36 which has a low coefficient of thermal expansion, $1.3 \text{ mm}/\text{m}/^\circ\text{C}$ (approximately 10 times lower than that of stainless

steel). The Invar plates are approximately 16-inch in height and 0.25-inch or 0.5-inch in thickness.

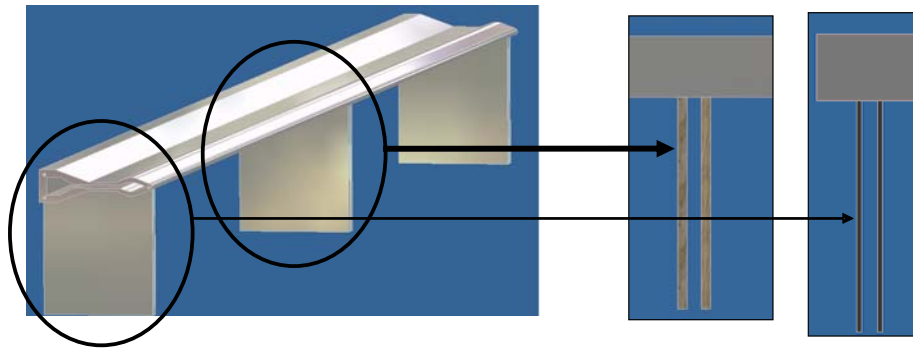


Fig.5.3 Vacuum chamber supports

5.3. Mechanical Stability of the Magnet-Girder Support System

a) Thermal Stability

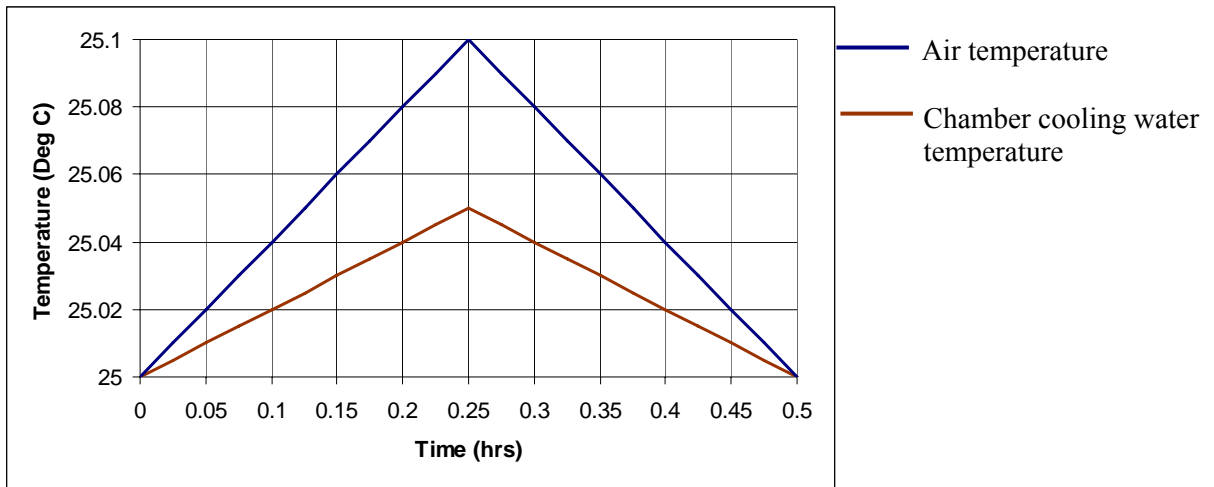


Fig.5.4 Fluctuations in the tunnel air temperature, and process water temperature

Fluctuations of the tunnel air temperature and process water temperature will result in displacements of both the magnets on the girders and the BPMs on the vacuum chambers. To insure acceptable thermal deformations of the ring components, process water and tunnel air temperature variations are specified to be within ± 0.05 °C and ± 0.1 °C respectively. One-hour cycles are specified for both the air and process water temperatures. To investigate the effect of temperature transients, FE thermal analyses were done for the girder, magnets and vacuum chamber assembly. For the analyses, the variations in the temperature of the tunnel air and the cooling water flowing through vacuum chamber were approximated by linear curves as shown in Fig. 5.4. A value of 8

$W/m^2 \text{ } ^\circ C$ and $15,000 W/m^2 \text{ } ^\circ C$ were assumed for air convection and water convection boundary conditions, respectively.

The advantage of insulating the girder on its thermal stability was investigated. A glass wool material with a thermal conductivity of $0.03 W/m \text{ } ^\circ C$ was considered. The analysis results, shown in Fig.5.5, indicate that by insulating the girder the thermal deflection can be minimized by a factor of 2. Similar findings for the effect of girder insulation have been reported in the experimental study of thermal deformation of the magnet girder at the SRRC storage ring [Ref.5.2], [Ref.5.3].

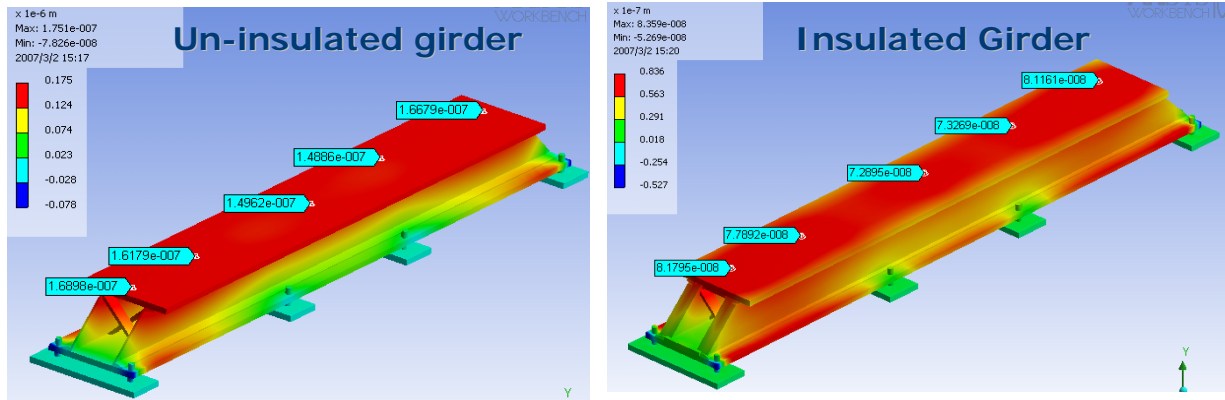


Fig.5.5 Contour plots showing deflection for (a) **Un-insulated girder**: Maximum thermal deflection = $0.17 \mu m$, and (b) **Insulated girder**: Maximum thermal deflection = $0.084 \mu m$.

Fig.5.6 shows the vertical displacements for the girder, magnets and vacuum chamber assembly due to time variation in the temperatures of the tunnel air and the cooling water flowing through the vacuum chamber. The results indicate that the maximum misalignment between the magnets is less than $0.03 \mu m$. For the vacuum chamber, at the points supported by the invar plates, the maximum vertical displacements are less than $0.15 \mu m$.

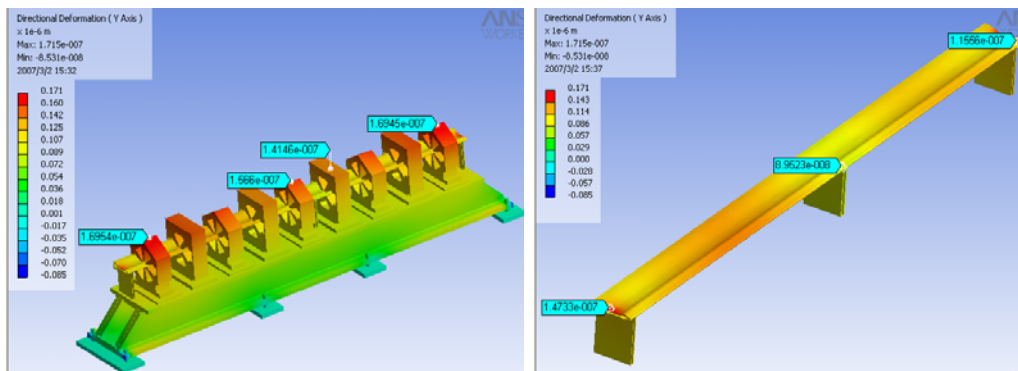


Fig.5.6 (a) Maximum vertical mis-alignment between the magnets $< 0.03 \mu m$, (b) maximum vertical deflection for the vacuum chamber at the BPM locations $< 0.15 \mu m$.

b) Vibration Stability

Sources that can induce mechanical vibrations in the girders magnets and vacuum chamber consist of turbulent flow in water cooling conduits and random ground motion. The effects of flow-induced vibrations can be minimized by paying close attention to several useful design guidelines, namely:

- 1) Locate all rotating equipments including fans, blowers, compressor, and pumps outside the storage ring tunnel, preferably tens of meters away from the tunnel flow and ceiling.
- 2) Keep low flow velocities (less than 2m/s) in the process water headers.
- 3) Design header supports to minimize their vibration, such as by integrating viscoelastic dampers in the headers hangers, or by attaching headers directly to the ceiling.
- 4) Arrange water flow circuits and connection fittings such that sharp bends are eliminated. Special attention is to be given to the routing and clamping of the hoses and tubes that connect the magnets and vacuum chambers to their respective headers.

The random ground motion can be affected by several sources, such as compressors, rotating machinery, traffic and other “cultural noises”. Fig.5.7 shows a comparison between the PSDs of the random ground motions near the NSLS-II site at the CFN building, at an NSLS beamline and at free field between NSLS and CFN.

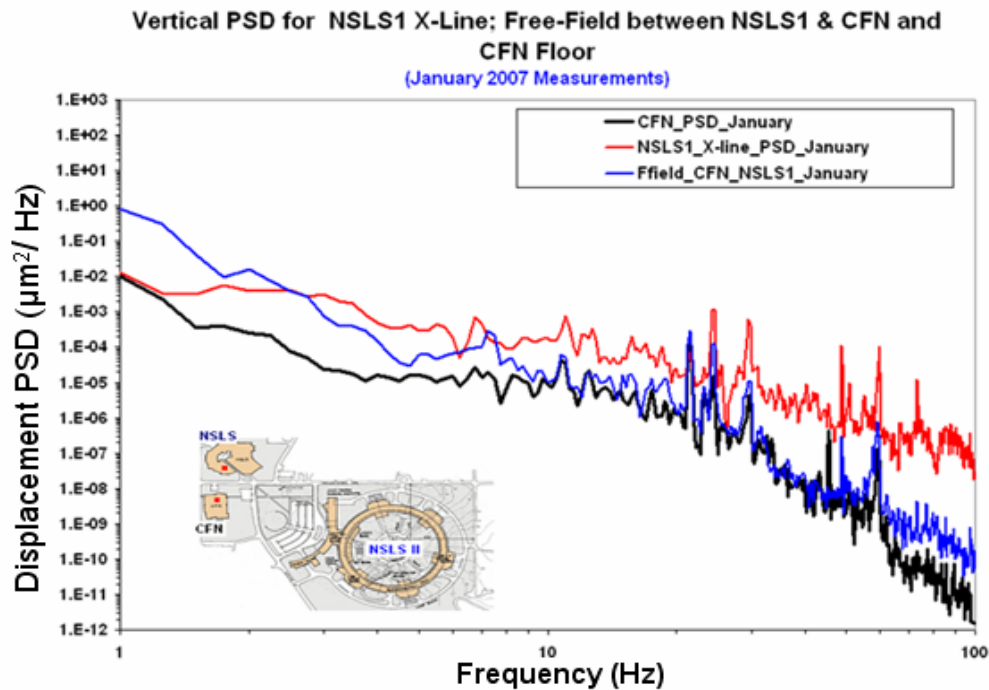


Fig. 5.7 Displacement PSDs at locations near the NSLS-II site [Ref. 4].

These PSDs compare favorably with those obtained at most of the light sources except for three peaks between 20-30 Hz from local noise sources. The RMS displacement at the CFN floor is approximately 20 nm (2-50 Hz), which indicates that the NSLS-II floor specification of 25 nm (4-50 Hz) is easily achievable. As expected, the ambient ground motion drops off sharply with frequency. There is considerably ground motion in the low frequency range, for instance, approximately 200 nm rms in 0.5-4 Hz band. However, the floor motion of the storage ring in this low frequency range is expected to be highly correlated since the wavelength of the Rayleigh waves in concrete is greater than 600 m for frequencies lower than 4 Hz. Relaxed tolerances (yet to be specified) for such correlated motions are expected to be easily met with the use of real-time orbit feedback system. For frequencies greater than 50 Hz the rms ground motion is too small to have a significant effect on beam stability even if it is amplified by the girder assembly. Thus, the design goal for the girder support system is to have its first lowest natural frequency of greater than 50 Hz.

Finite element modal analysis of the NSLS-II 5.7-m girder and magnets assembly shows that the lowest two natural frequencies of the system are 63 Hz and 79 Hz. The corresponding mode shapes, rolling and twisting of the girder, are depicted in Fig.5.8. (Note: To include effect of Bellville washers for the end pedestals as explained in Sec.5.2, the Young's modulus of the end pedestals were assumed to be 10 times lower than that for the central pedestals.)

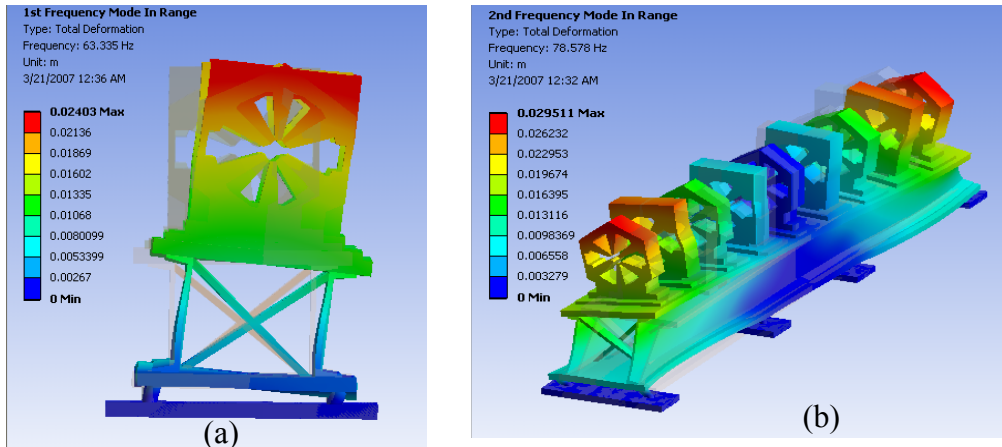


Fig.5.8 Natural modes of vibration for the girder-magnets assembly: (a) rolling mode = 63 Hz, (b) twisting mode = 79 Hz

To get a better handle on forecasting the response of the girder, magnets and vacuum chamber assembly to ambient ground vibration, a random vibration analysis was carried out. The random ground motion data is provided as a power spectrum input loading to the finite element model of the assembly. Fig. 5.9 shows the FEA one-sigma displacement result in the vertical direction for the girder-magnets-chamber assembly. For a random ground motion that has RMS amplitude (2-50 Hz) of 20 nm, the following results are obtained: (a) the maximum random displacement of the chamber within one

standard deviation will be ~ 26 nm, and (b) The maximum random displacement of the girder and magnets, within one standard deviation will be ~ 21 nm.

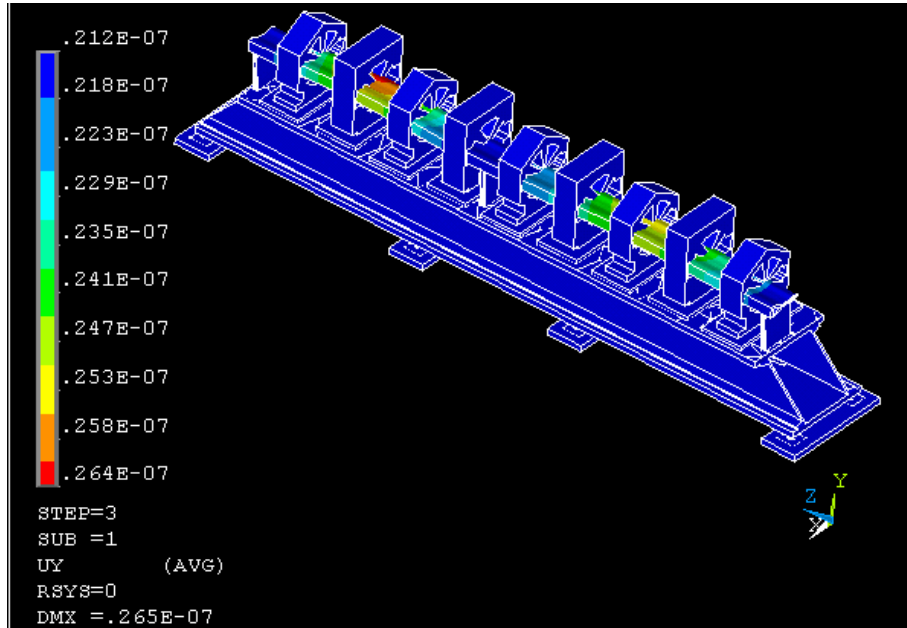


Fig. 5.9 One-sigma displacements in the vertical direction for the girder-magnets-chamber assembly

5.4. Mechanical Stability of User BPMs and X-BPMs

BPMs at the two ends of the insertions devices (user BPMs) and X-BPMs in the front ends have more stringent mechanical stability requirements. The vertical and horizontal rms displacements are specified to be less than $0.1 \mu\text{m}$ and $1 \mu\text{m}$, respectively. We have investigated BPM support stands made from carbon fiber composites to meet the tight tolerance in the vertical direction. A carbon fiber composite can have thermal coefficient of expansion as low as $0.1 \mu\text{m}/\text{m}/^\circ\text{C}$. With the tunnel air temperature fluctuations controlled to within ± 0.1 $^\circ\text{C}$, the vertical displacement 1 m high support stand can be maintained to about $\pm 0.01 \mu\text{m}$.

The carbon fiber composites are, however, weak in the transverse (thickness) direction. Typical Young's moduli along the principal and transverse directions are 120 GPa and 7.5 GPa, respectively. A random vibration analysis was performed to calculate the rms displacement of a support stand under typical ambient floor motion. The support stand is made from two commercially-available carbon fiber composite tubes of 6-inch diameter and 1/8-inch thickness. The weight of the user BPM assembly was assumed to be 10 Kg.

Fig. 5.10 (a) shows displaced shape of the support stand. Displacement PSDs of the base and the BPM assembly are depicted in Fig. 5.10(b). The rms displacement (2-50 Hz, 1σ) is calculated to be 0.06 μm which is well within the specification of 1 μm .

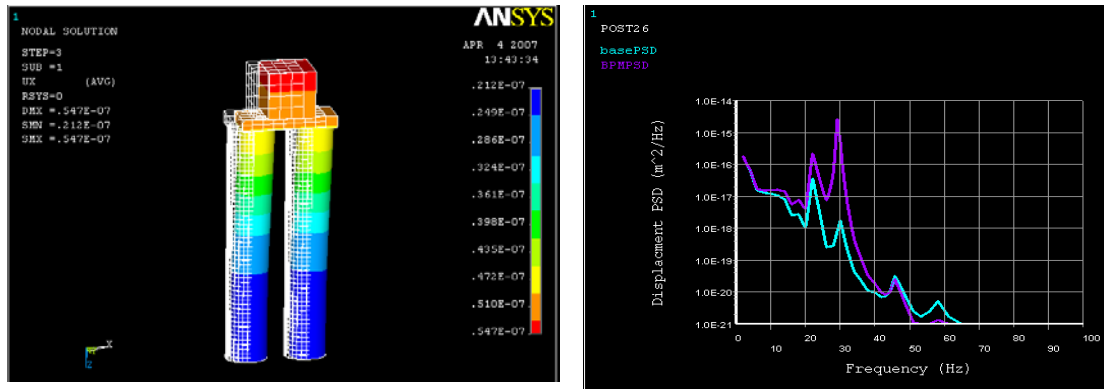


Fig. 5.10 (a) FE model of a carbon fiber composite support stand, (b) displacement PSDs of the base (blue curve) and the BPM assembly (magenta curve).

A thermally-insulated support stand made from structural steel, similar to the one in use at APS, was also investigated as a cost-effective alternative, especially for the considerably heavier X-BPM assembly. A 10-inch diameter, $\frac{1}{4}$ -inch thick structural steel pipe filled with sand and insulated by 2-inch thick mineral wool insulation was used for the FE model. A maximum temperature rise of 0.003 $^{\circ}\text{C}$ was obtained at the two end of the pipe for the air temperature fluctuation shown in Fig. 5.4. With an average temperature rise of only about 0.001 $^{\circ}\text{C}$, the thermal deformation at the top of the stand is limited to about 0.013 μm .

The first natural frequency of the steel support stand with 30 kg of the BPM assembly is 78 Hz in the transverse direction. Consequently, there is essentially no amplification of the ambient floor motion in the vertical direction, and only a small amplification in transverse direction, from 20 nm to 22 nm. The sand-filled, thermally insulated steel pipe can therefore, meet all design specifications with comfortable margin.

References

- [Ref.5.1] R.O.Hettel, "Beam Stability at Light Sources," Review of Scientific Instruments, 73, March 2002, pp.1396-1401
- [Ref.5.2] D.J. Wang, H.C.Ho, C.K. Kuan and J.R. Chen, "Experimental Study of Thermal Deformation of the Magnet Girder at SRRC Storage Ring," Proceeding of APAC 2001, Beijing, China, 2001.

- [Ref.5.3] J.R. Chen, D.J. Wang, Z.D. Tsai, C.K. Kuan, S.C. Ho, J.C. Chang, “Mechanical Stability Studies at the Taiwan Light Source,” MEDSI 2002, APS, Argonne ,IL, Sept.5-6, 2002.
- [Ref.5.4] Verbal communication with N. Simos, Experimental ground motion data measured by N. Simos at various BNL locations.

6. Orbit Feedback

To realize the benefits of the high brightness and small beam sizes of NSLS-II, it is essential that the photon beams are exceedingly stable in position and angle. We shall require beam motion of no more than 10% of beamsize or angular spread. Ideally, the spatial and angular stability of the electron beam should be maintained for at least the duration of spectral scans, which typically run from a few ms to a few hours. Since the minimum vertical beta function is about 1 m, when we take the vertical emittance as $10^{10}/4\pi$ m, the vertical beamsize is $2.7 \mu\text{m}$ rms. Therefore, we require the beam position stability to be $\sim 0.3 \mu\text{m}$ in the short straight sections.

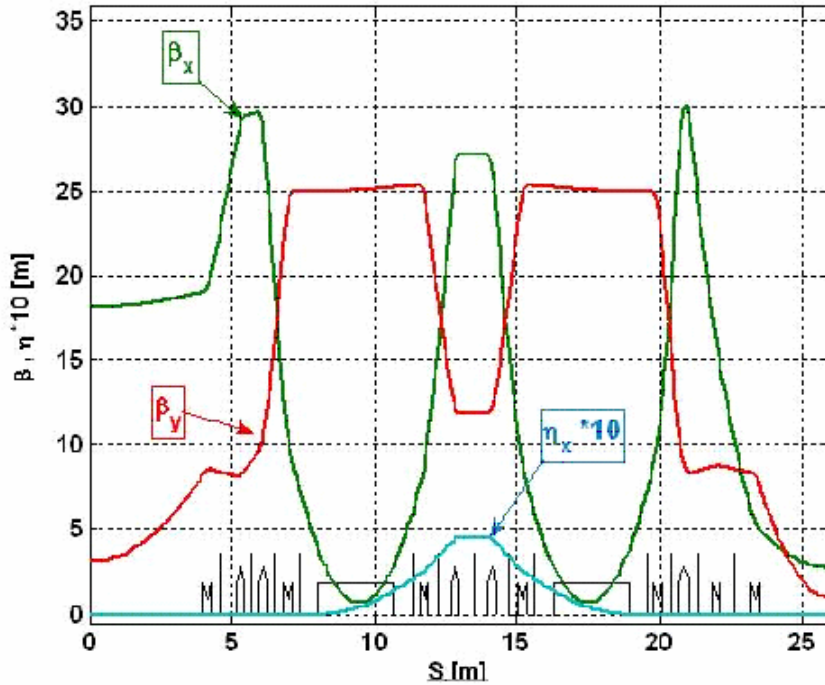


Figure 6.1: Lattice functions for one-half superperiod of DBA-30 lattice as specified in the CDR.

The lattice functions for the NSLS-II storage ring design as presented in the Conceptual Design Report (December 2007) are shown in Figure 6.1. For this lattice, we have calculated the performance of a fast, closed-orbit feedback system with 120 BPMs and 120 correction trims. To illustrate the system performance, we translated the quadrupoles randomly and independently according to a distribution with $1 \mu\text{m}$ rms and also varied the transverse position of the BPMs by $1 \mu\text{m}$ rms. We then averaged over an ensemble of 400 such configurations of random displacements. The resulting beam rms motion $\sigma_{\Delta y}$

is shown in blue in Figure 6.2. We see that it is well-approximated by the function $14\sqrt{\beta_y[m]}\mu\text{m}$, which is shown in green.

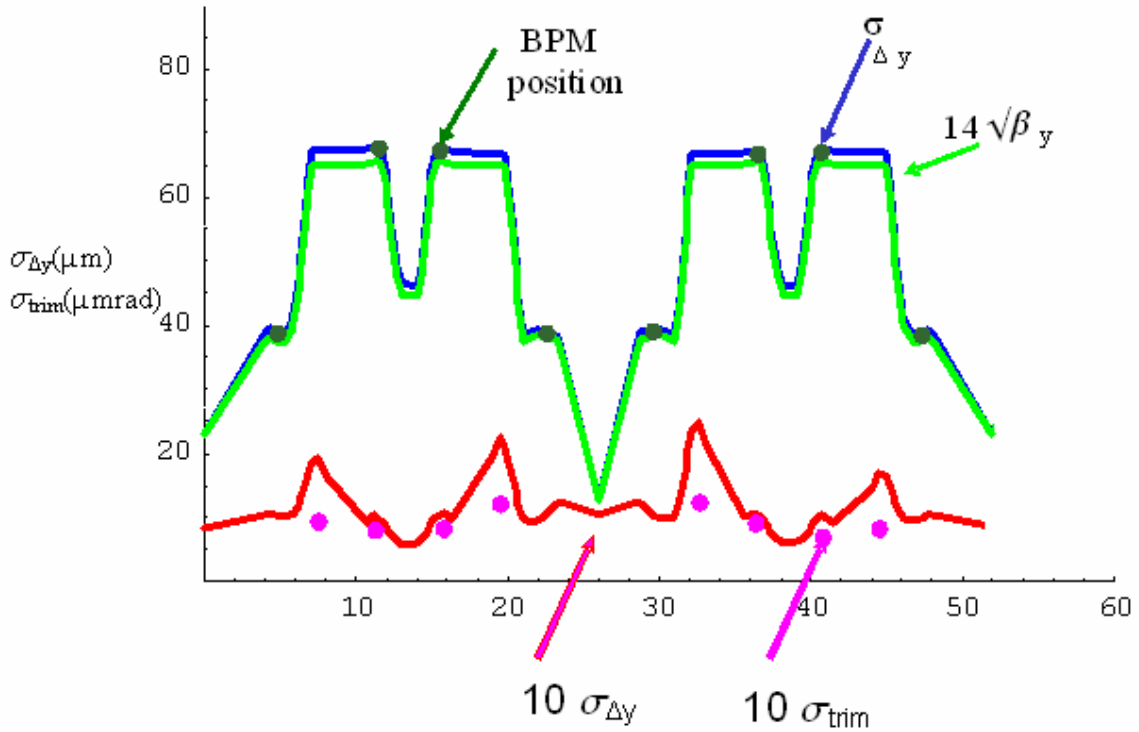


Figure 6.2: Illustration of feedback system performance correcting the orbit resulting from $1\mu\text{m}$ rms random displacement of the quadrupoles. The orbit correction uses 4 BPMs and 4 trim dipole correctors. The blue curve shows the uncorrected orbit and the red curve is 10 times the corrected orbit. The purple dots indicate ten times the strength of the correction magnets in μrad .

For each set of Gaussian random errors for the quadrupole and BPM vibration (with rms displacement of $1\mu\text{m}$), we calculated the open-loop BPM signal, then used the single-value-decomposition (SVD) matrix to calculate the corrector strength, and finally calculated the orbit with the feedback loop closed. After averaging over 400 random samples, we obtained the residual RMS beam motion.

In Fig. 6.2, to allow the residual orbit (red curve) to be seen, we multiplied it by a factor of 10. The height of the purple dots represents 10 times the rms strength of the correctors, in units of μrad . The figure shows that the feedback loop reduces the beam motion at the center of the long straight section ($z = 0$) from $25\mu\text{m}$ to $0.7\mu\text{m}$. The maximum RMS corrector strength is on the order of $1.2\mu\text{rad}$. We conclude from these calculations that a feedback system utilizing 4 correctors and 4 BPMs can reduce the orbit motion

sufficiently to meet our goals. We plan to hold the BPMs fixed vertically to $0.1 \mu m$ and horizontally to $1 \mu m$, in order to meet the electron beam stability tolerances in the short straight sections.

The beam motion due to power supply noise in a digital feedback system is determined by the voltage corresponding to the last bit of the power supply and the power supply current noise itself. We find that if we require beam motion at the beam waist where $\beta_y = 1 \text{ m}$ to be less than $0.3 \mu m$, the RMS trim noise should be less than 10 n-rad. The specification for the corrector magnet power supplies is to provide $0.01 \mu rad$ resolution of the last bit and a noise level below $0.003 \mu rad$.

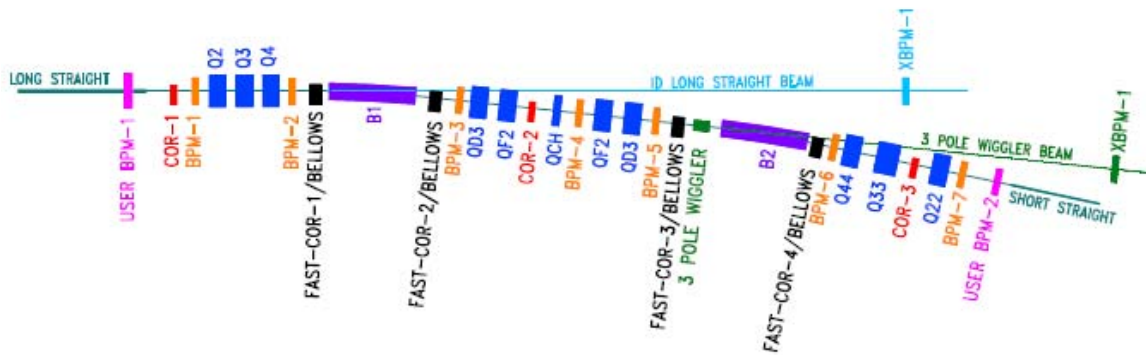


Figure 6.3: Schematic showing the position of the correction dipoles and the BPMs in one-half superperiod. This is the current lattice updated from that discussed in the CDR. In particular, the position for three-pole wigglers in the dispersive region is shown.

The quadrupoles and sextupoles will be aligned on girders to better than $50 \mu m$, and girders will be aligned relative to each other to better than $100 \mu m$. Beam based alignment will be used to calibrate the BPMs relative to the quadrupoles and sextupoles. The orbit correction system contains 7 correction magnets and 7 BPMs per half-superperiod as illustrated in Fig. 6.3. It has the capability of correcting the misalignment expected during first commissioning of the storage ring as well as for the long-term settlement of the concrete floor.

A subset of 4 correction magnets located over stainless steel bellows (to reduce eddy current effects) will be used in the feedback system. Use of 4 BPMs appears to be sufficient but we have the capability of using more than 4 if future considerations indicate that this is desirable. User BPMs on carbon-composite supports will be installed in straights having insertion devices, to provide the highest degree of thermal stability of the BPM position. We plan to incorporate x-ray BPMs located on the experimental beamlines into the orbit feedback system in order to improve angular stability. Only x-ray BPMs located before any optical elements will be feedback to the electron beam. X-ray BPMs located after optical elements can be used for feedback control of hardware in the experimental end-station. At this time we do not plan on using local feedback systems; however this option is not precluded if it is found to be beneficial.

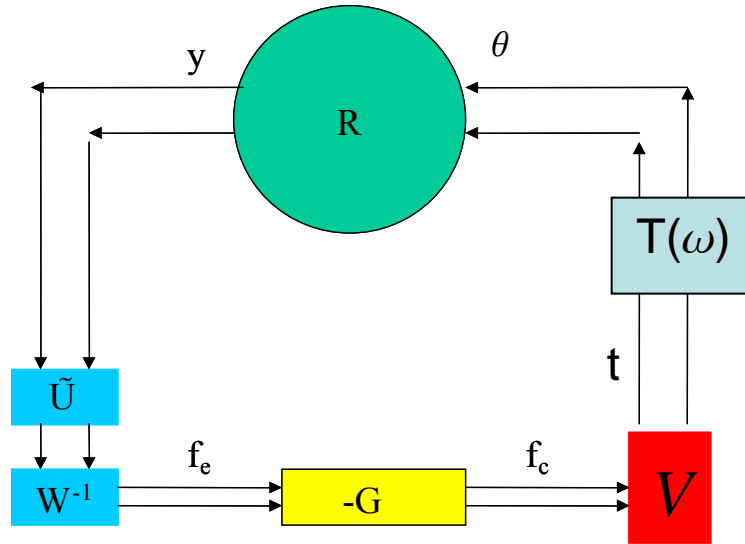


Figure 6.4: Schematic of the closed orbit feedback system based on single value decomposition of the response matrix.

A schematic of the orbit feedback system is presented in Fig.6.4. The response matrix R , between the corrector excitation and the orbit displacement at the BPMs, can always be decomposed in the form $R = UV\tilde{W}$, such that W is diagonal. Each eigenvector corresponds to an independent channel. The negative feedback gain G and the frequency response $T(\omega)$ are also diagonal. U and V are orthogonal with orthonormal columns (not necessarily square matrices). G is chosen to be large and positive and at low frequency the error signal is reduced by $1+G$. At higher frequency $T(\omega)G$ is complex and the system has to be carefully designed to avoid oscillation. In this regard, it is very important that all the correction magnets (including the effects of eddy currents in the chamber) have the same frequency dependence.

7. Electrical Systems

7.1 Global Beam Position System

A simplified block diagram of the global beam position system is in Figure 7.1. The BPM requirements will be discussed in the instrumentation section. The planned system will have all BPM data transferred to a single process where the corrector strengths will be calculated. The corrector strengths will then be transferred to the individual power supply interface. Both slow/alignment and fast corrections will be calculated in this process. The global timing system will supply synchronized triggers for the system. The overall throughput of the system is ~ 5 kHz.

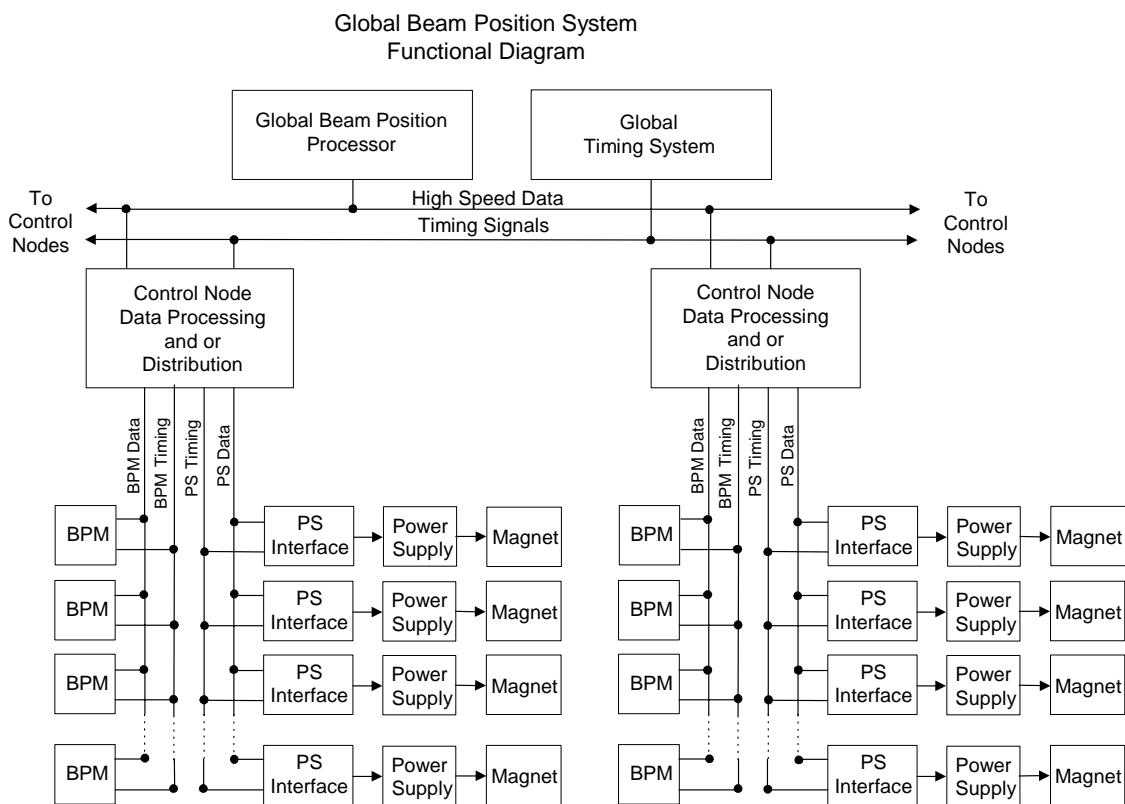


Figure 7.1: Block diagram of global position system.

A more detailed design of the system needs to be done. Some critical items that need to be investigated are the following:

1. The methods of data transfer between the various elements of the system.
2. The number of bpm and ps interfaces that are connected to a control node.
3. The data throughput of the overall system.
4. The choice of the process platform that meets calculation speed requirements.

7.2 Corrector magnets and power supplies used for global beam position system

The system will use 120 corrector magnets with separate horizontal and vertical coils. The magnets will be designed for fast correction of ~ 100 Hz. The dc transfer function of the magnet is $1000 \mu\text{rad}$ per 19.2 Amps. The magnets will be located over stainless steel bellows and or flanges. This is to minimize the affect of eddy currents of low resistance beam chambers, like aluminum that will decrease the effective bandwidth of the system. The magnets are placed at the ends of each main dipole magnet. There will be 120 horizontal and 120 vertical power supplies. These corrector magnets and power supplies will be also used in slow and alignment corrections. The power supplies will have a high current requirement for slow/alignment corrections and high voltage requirements for fast corrections.

The power supply requirements from accelerator physics are the following:

Frequency	Strength - RMS
< 5 Hz	800 μrad
20 Hz	100 μrad
100 Hz	10 μrad
1000 Hz	1 μrad
Resolution of last bit: 0.01 μrad	
Noise Level : 0.003 μrad (~ 4 ppm of 800 μrad)	

These rating are for vertical correction and the horizontal correction is less stringent and they need to be quantified.

The present plan for the corrector magnets power supplies are to use a four quadrant switch-mode class D amplifier. This will be able to meet the high current and high voltage requirement in an efficient topology. The amplifier will be incorporated into a bipolar current regulated power supply. The small signal bandwidth of the power supply will be ~ 2 kHz. A possible problem with this power supply will be from current ripple from the switching frequency. The plan is to use an amplifier that has a switching frequency of 81 Hz. which should give a small ripple current of ~ 2 ppm. The plot in figure 7.2 is the maximum fast correction strength the power supply can do before it is limited by its maximum voltage or current.

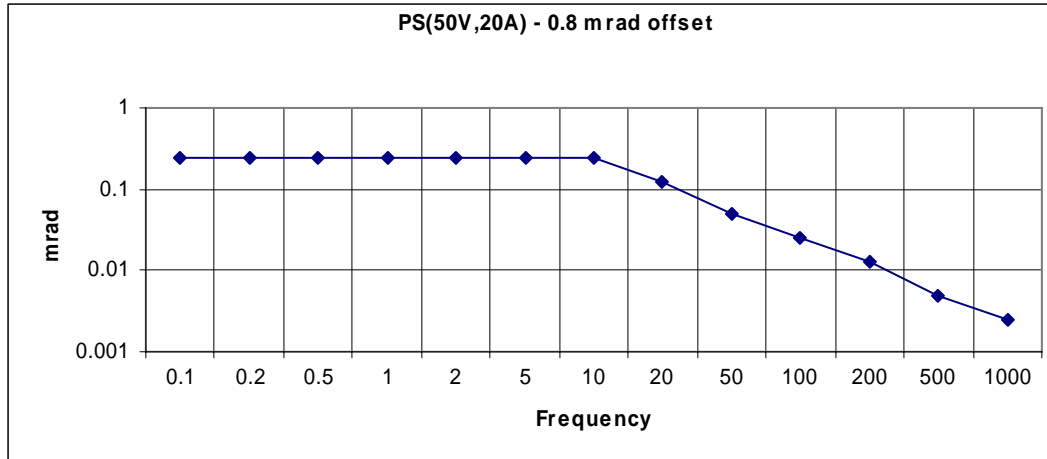


Figure 7.2: Peak corrector strength as a function of frequency for a corrector at a fixed offset of 800 μ rad for a bipolar power supply with a rating of 50 volts and 20 amps.

To get the resolution of 0.01 μ rad it is planned to use two 16 bit DACs in the power supply interface. One will be used for the slow large strength correction and the other for the fast smaller strength correction. The output of the DACs will be summed at different gains. The gain difference will be 4 which will give an effective resolution of 18 bits or ~ 0.003 μ rad.

The following is the planned R&D for corrector power supplies and magnets:

1. Measure the magnet field of a proto-type corrector magnet as a function frequency. These measurements will include transfer function and multi-poles.
2. Design and build a proto-type corrector power supply measure the frequency response of the current regulator.
3. Measure the current ripple of the power supply and overall current noise.

7.3 Power Supplies

(a) Main Dipole

The power supply is a unipolar, 2-quadrant, current-regulated supply. It will use two 12-pulse SCR converters in series with the center point connected to ground. This configuration will reduce the voltage to ground at the magnet load and reduce the voltage rating on various converter components. Each converter will have a two-stage LCRL passive filter and a series pass active filter. This is required to reduce the ripple current to low levels.

Each main dipole magnet has a bending angle of 0.1047 rad. The CDR has the current ripple spec. (referred to I_{max}) of 5 ppm for freq. 60 Hz and greater. This gives a ~ 524 nrad noise in the horizontal direction. (Assuming all the ripple current goes into the field.) The current ripple estimate may be reduced when a more thorough electrical circuit model is made for the dipole power supply. Also transmission line effects will have to be calculated.

CDR has the following power supply parameters:

resolution of reference current	18 bit \pm 1LSB
stability (8 h-10 s) – referred to I _{max}	40 ppm
stability (10s-300 ms) – referred to I _{max}	20 ppm
stability (300 ms- 0 ms) – referred to I _{max}	10 ppm
absolute accuracy – referred to I _{max}	100 ppm
reproducibility long term – referred to I _{max}	50 ppm

Redundant DCCTs will be used to confirm the power supply current reproducibility. High-precision DMMs and scanners will be used to monitor the power supply current, a redundant current sensor, and the analog current set point. This equipment will ensure long-term stability and reproducibility

(b) Multipole (Quad. & Sext.)

These circuits will use one power supply for each magnet. The power supply is a unipolar, single-quadrant, current-regulated switch-mode design. The power section is a commercial voltage-controlled switch-mode programmable power supply with high output bandwidth (~ 1 kHz). The power supply will use a DCCT as the current feedback device. To minimize current ripple, an additional output filter will be used. The CDR has the current ripple spec. (referred to I_{max}) of 15 ppm for freq. 60 Hz and greater.

CDR has the following:

resolution of reference current	16 bit \pm 1LSB
stability (8 h-10 s) – referred to I _{max}	200 ppm
stability (10s-300 ms) – referred to I _{max}	200 ppm
stability (300 ms- 0 ms) – referred to I _{max}	100 ppm
absolute accuracy – referred to I _{max}	200 ppm
reproducibility long term – referred to I _{max}	100 ppm

Like the main dipole redundant DCCTs will be used to confirm the power supply current reproducibility. High-precision DMMs and scanners will be used to monitor the power supply current, a redundant current sensor, and the analog current set point. This equipment will ensure long-term stability and reproducibility.

The R&D for the multipole power supplies is to build a proto-type and confirm the accuracy, stability, and current ripple of the power supply.

7.4 Beam Position Monitors

Libera Electron utilizes digital signal processing and enables accurate beam position monitoring, trouble-free commissioning, and local and global feedback building. When input signal levels are from around -35 dBm to 0 dBm the resolution is constant due to prevailing influence of phase noise. For the BPM buttons located on the 25 mm radius the r.m.s. uncertainty in 1 kHz bandwidth of beam position is around 0.5 microns. The

processing module is expected to have 2.5 microns 8-hour stability (with ambient temperature variation below 1°C), and temperature drift is expected to be 0.5 $\mu\text{/}^\circ\text{C}$.

With fast serial links, powerful FPGA and embedded CPU Libera Electron provides basis for orbit feedback building, with control system integration moved from the driver/backplane level to the network and transport layers.

As a result of mechanical, thermal and electronic drifts high pointing stability of the SR beam will be hard if possible to achieve utilizing only RF BPMs, which are located very close to the source point. Utilizing photon BPMs placed in the user beamline at significant distance allows to achieve the beam stability goals. Regular photon BPMs are based on measuring of the photocurrent from the blades made of refractory material and intercepting part of the photon flux from the insertion device or bending magnet. As it was demonstrated at APS with such BPMs it is possible to reach sub-microradian pointing stability, but at the expense of utilizing feedforward look-up tables to subtract predetermined offsets from the photon BPM readings as the ID gap varies. However, elevated noise/signal ration prevents using blades with large gaps. To overcome drawbacks pertinent to photoemissive photon BPM is was suggested by G. Decker et al. to employ back fluorescent BPMs. The horizontal fringes of the photon beam strike the copper target, which re-radiates fluorescent photons of approximately 8 keV energy. A set of four p-i-n diode detectors located above and below midplane then detect the fluorescence. Such BPMs are less sensitive to the stray synchrotron radiation from the elements of the ring and demonstrated high stability when intensity of the photon beam varied by factor of million. Such devices will be considered for utilization as well.

8. RF System

The electron beam longitudinal phase space is determined by the RF cavity fields and the interaction of the electron beam with impedances in the ring. Jitter in the RF cavity fields can cause energy or phase jitter of the electron beam. This can transform into transverse beam size or jitter by increasing the effective emittance and through dispersion.

The electron beam can interact with impedances in the ring causing intra and coupled bunch energy and phase oscillations leading to emittance dilution and transverse beam motion through dispersion. In the following sections tolerances on the phase and amplitude jitter will be derived from user requirements and causes of RF system amplitude and phase noise will be described.

8.1 RF tolerances imposed by user experiments

Timing experiments, such as the IR experiments run at NSLS currently, require that the timing jitter of the bunch be less than 5% of the RMS bunch length over the frequency range of 500 Hz to 50 kHz. This corresponds to a phase error of 0.1 degree for a 10 ps bunch, or a corresponding momentum jitter of 0.005%.

The majority of users are not concerned with timing experiments but require small and stable photon beam size. The vertical photon beam divergence for a experiment using a higher harmonic of an Insertion Device (ID) is given by¹

$$\sigma_{y'}^2 = \frac{\lambda_n}{2L} \sqrt{1 + 16n^2 N_w^2 \sigma_\delta^2} + \frac{\varepsilon_y}{\beta_y} \quad (1)$$

Where n is the harmonic of the ID being used, N the number of periods, L the length of the ID, σ_δ the momentum deviation, ε_y the vertical emittance of the electron beam and β_y the vertical beta function of the lattice at the insertion device location.

For NSLS-II $\varepsilon_y \sim 8 \times 10^{-3}$ nm-Rad and $\beta_y \sim 1$ m at the ID straights, $L \sim 3$ m, $N \sim 100$. Because of the n^2 dependence, the worst case is for $n \gg 3$ where the two terms on the right hand side of equation (1) are comparable. Thus using (1) for a 10 % increase in beam size the momentum jitter must be 40% of the inherent momentum spread, or equivalently a phase jitter of 1.2 degrees.

A third limit on momentum spread is due to longitudinal energy oscillation leading to filamentation and increase in beam size. With a momentum kick $\Delta p/p$ to the bunch, an electron would have a longitudinal oscillation

$$\delta(t) = (\Delta p / p) \sin \nu_s \omega_0 t + \delta_0 \sin \nu_s \omega_0 (t + t_0).$$

Because of the longitudinal tune spread the two terms will decohere and become

$$\delta(t) = (\Delta p / p) \sin \nu_s \omega_0 (t + t_1) + \delta_0 \sin \nu_s \omega_0 (t + t_2)$$

where t_1 and t_2 are two random numbers. Averaging over t_1 , t_2 and δ_0 we arrive at

$$\sigma_\delta = \sqrt{\frac{1}{2} (\Delta p / p)^2 + \sigma_{\delta,0}^2} = \sqrt{1 + \frac{1}{2} f^2 \sigma_{\delta,0}^2}$$

where $f = (\Delta p/p)/\sigma_\delta$ is the relative kick factor. For a 10% increase in σ_δ , $f \sim 0.65$ or $\Delta p/p = 6.5 \times 10^{-4}$. The corresponding phase jitter is given by $\Delta\phi = \frac{h\alpha_c}{\nu_s}(\Delta p/p)$ where h is the harmonic number (1300), α_c is the momentum compaction factor = .00037 and $\nu_s \sim 0.01$, $\Delta\phi = 1.8$ degrees.

The transverse electron beam size and position is related to the momentum spread and average momentum respectively. The beam size is given as $\sigma_{x,y} = \sqrt{\beta_{x,y}\epsilon_{x,y} + (\eta_{x,y}\sigma_\delta)^2}$. The residual dispersion η_y is of the order 1mm and the second term is negligible in beam size. Vertical position is given as $y = y_0 + \eta_y\langle\delta\rangle$. The allowed centroid jitter is 10% of the beam size or $0.3\mu\text{m}$, therefore the average momentum jitter should be less than 3×10^{-4} , with a corresponding phase jitter of 0.82 degrees.

The above limits are summarized in Table 8.1.

Table 8.1: Longitudinal beam stability requirements

	Phase jitter (°)	Momentum jitter ($\Delta E/E$)%
Timing-dependent experiments	0.1	0.005
Vertical divergence (from momentum jitter)	1.2	0.04
10% increase in σ_δ due to filamentation	1.8	0.065
Vertical centroid jitter	0.82	0.03

Due in large part to the near zero dispersion in the ID straights which mitigates the effect of momentum jitter, the tolerance on the RF is dominated by the IR timing experiments.

8.2 System contributions to RF amplitude and phase noise

The RF system can contribute to beam jitter both actively and passively. Noise injected into the RF system anywhere in the signal path can be amplified and superimposed on the RF cavity fields. In particular, broadband “white” noise of the master oscillator can excite synchrotron oscillations in the beam causing beam motion. Studies² have shown that this can be exacerbated by the Robinson frequency shift which shifts the beam frequency response toward lower frequencies. Since the master oscillator phase noise falls off exponentially, the beam response function maxima shifts towards higher noise levels. In addition to oscillator noise the system is sensitive to power supply noise. One candidate high power klystron has a RF phase variation vs. DC power supply (anode) voltage of 12 degrees / %V. The modern pulse-switch-modulation (PSM) power supply has typical noise/ripple performance listed in table 2.

Typical noise/ripple performance	
Full range	< 1 % pk-pk
75 V (0.138%)	From 1 kHz – 2 kHz
15V	From 2 kHz - 4 kHz
3 V	From 4 kHz – 12 kHz
50 V	For > 12 kHz

Table 8.2. THALES 54kV 12A PSM power supply

If left uncorrected, the power supply ripple would contribute 1.6 degrees of phase jitter. Feedback either around the klystron directly or including the cavity can bring this to acceptable levels.

The beam can interact with fundamental and higher order mode impedances causing instabilities. Initial studies show the beam to be longitudinally stable in the presence of the 500 MHz cavity system. Further studies are required for the landau cavity HOM's, whose 7k-ohm impedance would be unstable in the absence of the tune spread induced by the long bunches created by the combined 500MHz/1500MHz system.

This bunch-lengthening cavity also induces a phase shift of the bunches along the bunch train comparable to or exceeding the bunch length³, although no problems have been identified by user experiments yet.

The bunch is unstable in the presence of the rings transverse broadband impedances, and NSLS-II will require a transverse damper.

- 1) Weiming Guo, "Longitudinal beam parameter tolerances of NSLS-II" NSLS-II tech-note #0025
- 2) J. Byrd, "Effects of phase noise in heavily beam loaded storage rings" PAC 1999
- 3) N. Towne, "Bunch and RF Stability and RF Noise in NSLS-II" NSLS-tech-note #0027